iScience

CellPress
OPEN ACCESS

Article

Distinct Tissue Damage and Microbial Cues Drive Neutrophil and Macrophage Recruitment to Thermal Injury

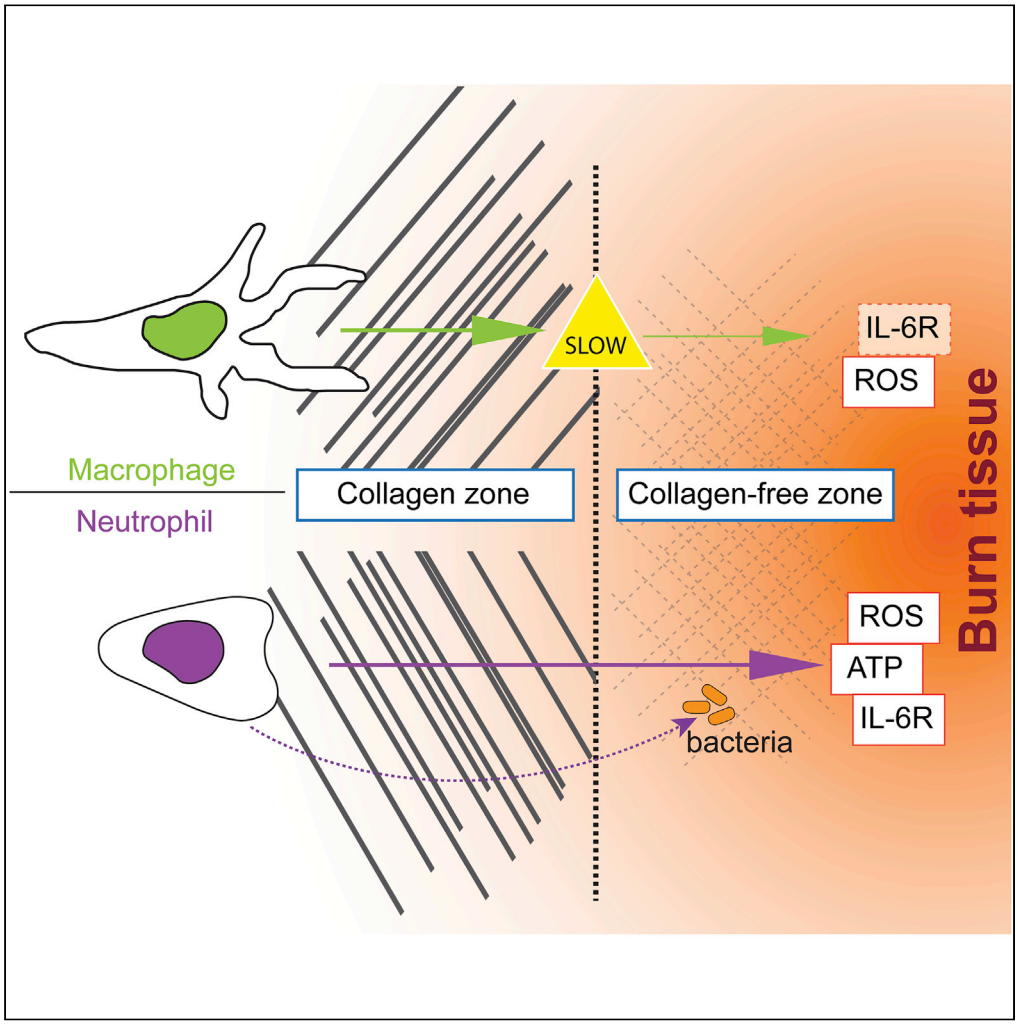

Francisco Barros-Becker, Jayne M. Squirrell, Russell Burke, ..., Kevin W. Eliceiri, Angela Gibson, Anna Huttenlocher

huttenlocher@wisc.edu

HIGHLIGHTS

Neutrophils, but not macrophages, rapidly migrate into a burn collagen-free zone

Lack of ATP or ROS affects neutrophil and macrophage recruitment distinctively

Absence of *Il-6r* strongly affects neutrophil recruitment to a sterile burn wound

Il-6r neutrophil recruitment defect can be rescued during *P. aeruginosa* infection

Barros-Becker et al., iScience *23*, 101699
November 20, 2020
https://doi.org/10.1016/j.isci.2020.101699

iScience

CellPress
OPEN ACCESS

Article

Distinct Tissue Damage and Microbial Cues Drive Neutrophil and Macrophage Recruitment to Thermal Injury

Francisco Barros-Becker,[1,2,8] Jayne M. Squirrell,[3,8] Russell Burke,[1] Julia Chini,[1,6] Julie Rindy,[1,4] Aos Karim,[5] Kevin W. Eliceiri,[3,7] Angela Gibson,[5] and Anna Huttenlocher[1,4,9,*]

SUMMARY

Tissue damage triggers a rapid innate immune response that mediates host defense. Previously we reported that thermal damage of the larval zebrafish fin disrupts collagen organization and induces a robust and potentially damaging innate immune response. The mechanisms that drive damaging versus protective neutrophil inflammation in interstitial tissues remain unclear. Here we identify distinct cues in the tissue microenvironment that differentially drive neutrophil and macrophage responses to sterile injury. Using live imaging, we found a motile zone for neutrophils, but not macrophages, in collagen-free regions and identified a specific role for interleukin-6 (IL-6) receptor signaling in neutrophil responses to thermal damage. IL-6 receptor mutants show impaired neutrophil recruitment to sterile thermal injury that was not present in tissues infected with *Pseudomonas aeruginosa*. These findings identify distinct signaling networks during neutrophil recruitment to sterile and microbial damage cues and provide a framework to limit potentially damaging neutrophil inflammation.

INTRODUCTION

Disruption of tissue homeostasis by damage triggers intricate and highly regulated tissue repair programs. Innate immune cells, including neutrophils and macrophages, are among the first responders to tissue damage and infection (de Oliveira et al., 2016). Macrophages clear damaged tissue and initiate tissue repair, whereas neutrophils, although necessary for host defense, can mediate damaging inflammation that delays wound healing and regeneration (Schofield et al., 2013). Innate immune cells rapidly mobilize to both sterile and infected tissues by sensing both soluble and insoluble cues that orchestrate the inflammatory response (Lämmermann et al., 2013; Niethammer et al., 2009; de Oliveira et al., 2014; Yoo et al., 2011). Complex injuries, such as burns, generate an abrupt remodeling of the tissue, accompanied by a rapid and long-lasting immune response (Miskolci et al., 2019). However, few studies have addressed the mechanisms of leukocyte recruitment to thermal injury and the cues that mediate potentially damaging inflammation (Karim et al., 2019a; Lateef et al., 2019).

Damage caused by thermal injury generates a high number of apoptotic and necrotic cells (Gravante et al., 2006a). This necrotic tissue, as well as the affected surrounding tissue, mediates the release of pro-inflammatory factors. Cell disruption releases a variety of Danger Associated Molecular Patterns (DAMPs), such as exposed DNA, reactive oxygen species (ROS), adenosine triphosphate (ATP), and N-formyl peptides (Bayliss et al., 2014; Rani et al., 2017; Shupp et al., 2010; Zhang et al., 2010). These factors, in turn, induce production of pro-inflammatory cytokines like tumor necrosis factor alpha (TNF-α), interleukin (IL)-8, IL-1β, and IL-6, which can sustain the inflammatory response (Rani et al., 2017; Rodriguez et al., 1993). Immediately following a burn injury, organized collagen is lost, innate immune cells migrate toward the damaged tissue, and tissue remodeling precedes tissue repair and regeneration (Lateef et al., 2019; LeBert et al., 2018; Miskolci et al., 2019).

Here, we take advantage of zebrafish larvae to examine the spatiotemporal events occurring during the innate immune response to burn wounds. We show that neutrophils infiltrate rapidly into a collagen-free zone after thermal injury, whereas macrophages infiltrate more slowly, in a two-step process. Furthermore, we identified distinct mechanisms of neutrophil and macrophage responses. Although IL-6 is known to

[1]Department of Medical Microbiology and Immunology, University of Wisconsin-Madison, Madison, WI, USA

[2]Cellular and Molecular Biology Doctoral Training Program, University of Wisconsin-Madison, Madison, WI, USA

[3]Laboratory for Optical and Computational Instrumentation, Center for Quantitative Cell Imaging, University of Wisconsin-Madison, Madison, WI, USA

[4]Department of Pediatrics, University of Wisconsin-Madison, Madison, WI, USA

[5]Department of Surgery, University of Wisconsin-Madison, Madison WI, USA

[6]School of Pharmacy, University of Wisconsin-Madison, Madison, WI, USA

[7]Department of Medical Physics, University of Wisconsin-Madison, Madison, WI, USA

[8]These authors contributed equally

[9]Lead Contact

*Correspondence: huttenlocher@wisc.edu

https://doi.org/10.1016/j.isci.2020.101699

mediate tissue inflammation, few studies have addressed its role in neutrophil recruitment. We identify a specific role for the IL-6 receptor in neutrophil, but not macrophage, motility and recruitment to sterile burn injury. Furthermore, we demonstrate that IL-6 receptor signaling is not necessary for neutrophil responses to thermal injury in the presence of a microbial cue.

RESULTS

Thermal Injury Triggers Distinct Neutrophil and Macrophage Responses

Our recent studies show that thermal injury causes more complex tissue damage and generates a differential immune response compared with the well-studied transection wound (Miskolci et al., 2019). In this current study, to better understand this more complex damage and immunological response, we imaged the tissue response to caudal fin thermal injury in live larvae. During the initial burn response, there were large-scale tissue morphology changes and some of the injured fins generated a tissue mass that detached from the fin within the first 24 h post burn (hpb) (Figure 1A). Additionally, within the first 6 h after burn injury, there was robust recruitment of both neutrophils and macrophages into the damaged fin. To further characterize the dynamics of the leukocyte response, we imaged live larvae from a double transgenic line *Tg(mpeg1:H2B-GFP/lyzc:H2B-mCherry)* that labels macrophage and neutrophil nuclei, permitting automated tracking (von Dassow et al., 2009; Miskolci et al., 2019; Yoo et al., 2012). After thermal injury, both neutrophils and macrophages migrated into the damaged tissue, with neutrophils infiltrating out to the wound edge (Figure 1A). However, macrophages did not migrate as far as neutrophils into the distal tissue during the early wound response (by 6 hpb), as assessed by measuring the distance that macrophages and neutrophils traveled beyond the distal end of the notochord (Figures 1B and 1C). These data suggest that neutrophils and macrophages exhibit different migration dynamics in burned tissue.

To better understand the recruitment of neutrophils and macrophages to thermal injury, we imaged *Tg(mpeg1:H2B-GFP/lyzc:H2B-mCherry)* larvae at a high temporal resolution (<2 min between time points) for the first 6 hpb (Video S1). Individual neutrophils and macrophages were tracked and migration speed was quantified as the immune cells migrated from the trunk of the larva into the wound area—defined as crossing the plane of the distal end of the notochord, with the time of crossing designated as t = 0 (Figures 1D–1F). Interestingly, although both neutrophils and macrophages reduced their average speed rapidly after crossing into the wounded area, macrophages showed a greater reduction in speed than neutrophils after entering the wound area (Figure 1G). Additionally, we quantified the residency of neutrophils and macrophages in the designated burn wound region over time using the cell track foot prints (Figures 1H and 1I). Cumulative tracks for both neutrophils and macrophages were quantified for three time periods during early burn response: 0–2, 2–4, and 4–6 hpb. The percentage area of the wound region occupied by the tracks was compared with a similar region of the trunk adjacent to the wound, as delineated by the end of the notochord (Figure 1H). Over time, there was an increase in wound residency of both neutrophils and macrophages relative to that in the trunk. However, the increased occupation of neutrophils in the wound area relative to the trunk during early burn wound responses is greater than that of the macrophages (Figure 1I). Overall, these data indicate that there is a strong recruitment of both neutrophils and macrophages but, in contrast to tail transection wounds, there appears to be a limitation in the migration of macrophages into the burn wound area that does not affect the migration of neutrophils. Taken together, these data support the idea that macrophages and neutrophils interact differently with the thermally damaged tissue *in vivo*.

Differential Neutrophil and Macrophage Residency in the Collagen Free Zone

One possible contributor to the differential movement of leukocytes into the burn wound is changes in tissue architecture. Therefore, we further characterized neutrophil and macrophage migration to thermal injury by imaging leukocyte responses in conjunction with Second Harmonic Generation (SHG) imaging to visualize collagen organization (LeBert et al., 2018; Miskolci et al., 2019). SHG combined with multi-photon based fluorescence imaging was performed on live larvae following thermal injury using the *Tg(mpeg1:EGFP)* and *Tg(mpx:EGFP)* zebrafish lines, both in *casper* backgrounds to avoid pigmentation. As we previously reported, organized collagen fibers are not detected in the burn wound area (Figures 2A and 2C) (LeBert et al., 2018; Miskolci et al., 2019). We defined three zones within the burn wound based on SHG imaging; collagen zone (undamaged fibers), edge of collagen (end of the collagen fibers), and collagen-free zone (no detectable collagen fibers) (Figures 2A and 2C, Video S2). Neutrophils and macrophages were followed after thermal injury within each zone over time. To determine whether there was a difference between the ability of neutrophils and macrophages to transit between the different tissue

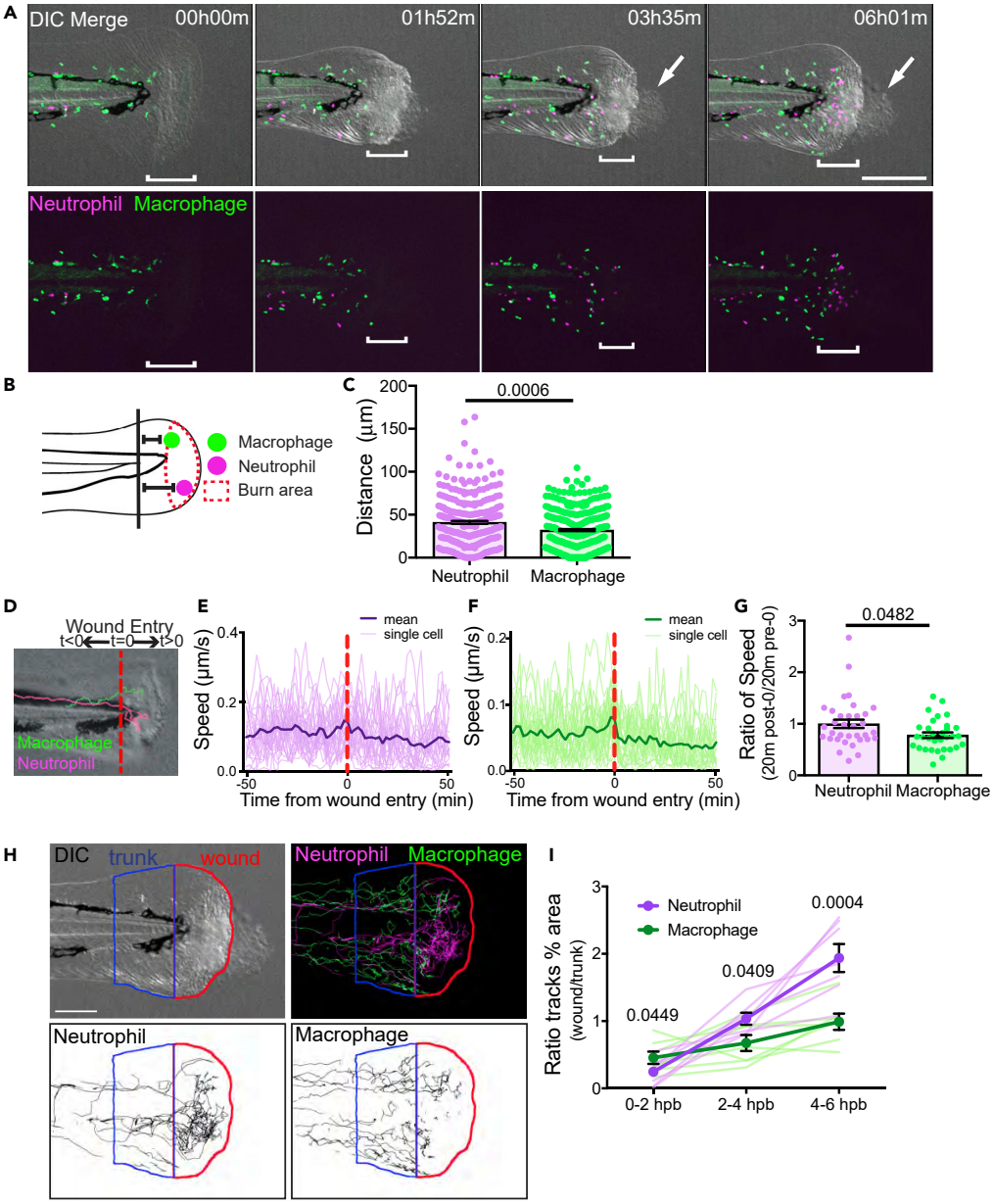

Figure 1. Leukocytes Exhibit Different Recruitment Kinetics to Thermal Injury

(A) Maximum intensity projection of confocal microscopy time-lapse stills of neutrophil (magenta) and macrophage (green) migration to burn wounds (DIC). Brackets indicate general burn region and arrows show the presence of the detaching tissue mass. t = 0 represents start of the recording, approximately 5 min following thermal injury. Scale bar, 200 µm.

(B) Schematic illustrating quantification of neutrophil and macrophage distance into the burn tissue. In the last frame of time-lapse recordings, the distance from the proximal edge of a cell nucleus to a line perpendicular to the posterior tip of the notochord was measured. Only cells posterior to the perpendicular line were quantified.

(C) Comparison of distance of single leukocytes from distal end of the notochord at 6 hpb. Symbols indicate individual cells.

(D) Tracks from 6 h time-lapse recordings were analyzed using automated tracking (Imaris). Diagram showing analysis method for assessing individual cell speed prior to ($t < 0$) or after ($t > 0$) entering into the burn wound zone ($t = 0$), delineated by red dashed line perpendicular to the distal tip of the notochord. Colored lines illustrate a single neutrophil track (magenta) and a single macrophage track (green).

(E) Instantaneous speeds, determined in Imaris, of individual neutrophils, with red dashed line indicating time ($t = 0$) when cell crossed into wound zone, as shown in (D).

Figure 1. *Continued*

(F) Instantaneous speeds, determined in Imaris, of individual macrophages, with red dashed line indicating time (t = 0) when cell crossed into wound zone, as shown in (D). Dark lines indicate arithmetic mean.

(G) Comparison of the ratio of the average speed during the 20 min following t = 0 to the 20 min preceding t = 0 of individual neutrophils (magenta) or macrophages (green). Symbols indicate individual cells.

(H) Tail fins were divided into trunk (blue) and wound (red) zones, delineated by the distal end of the notochord. Images of the cumulative automated neutrophil (magenta) and macrophage (green) tracks for 2 h time intervals for each cell type were converted to binary (lower images) and the percentage area occupied by those tracks was determined. Scale bar, 100 μm.

(I) Comparison of the ratio of the percentage of area occupied by tracks in the wound zone to the percentage of area occupied by tracks in the trunk zone at three time intervals. Symbols and corresponding dark lines represent arithmetic mean with SE. Pale lines represent individual larvae. Graphs (E)–(G) and (I) represent two independent experiments. Graphs (C) and (G) columns are arithmetic mean with SE. Additional statistical values in Table S1. See also Video S1.

microenvironments, we measured the total leukocyte volume as a tool to quantify changes in cell density over time at the collagen edge and the collagen free zone (Figures 2B and 2D). Additionally, these location-dependent differences in leukocyte residency between neutrophils and macrophages were further delineated by quantifying the change in residency during different time windows following thermal injury (Figure 2E). Neutrophils readily migrated into the collagen-free zone, reaching a peak of recruitment around 4.5 hpb (Figures 2B and 2E). After 6.5 hpb, neutrophils began leaving the collagen-free zone. The volume of neutrophils at the edge of the collagen zone remained relatively constant over time, suggesting that there was no major impediment to their movement into or out of the collagen-free tissue region (Figures 2B and 2E). However, macrophage recruitment to the collagen-free zone was reduced compared with neutrophils (Figures 2D and 2E), with peak recruitment after 15 hpb. Furthermore, macrophages accumulated at the edge of the collagen, compared with the collagen-free zone, suggesting that macrophages paused at the edge of the collagen before infiltrating the collagen-free area (Figure 2D). Additionally, following entry into the collagen free zone neutrophil morphology did not seem to be altered while macrophage morphology changed from elongated to more round (Figures S1A and S1B). These data suggest that changes in the tissue microenvironment induced by specific types of damage differentially influence the behavior of neutrophils and macrophages.

Neutrophil and Macrophage Recruitment to Thermal Injury Depends on Different Chemotactic Cues

Compared with excision wounds, burn wounds elicit a stronger and more prolonged immune response (Miskolci et al., 2019; Valvis et al., 2015). Mammalian burn injuries have zones of high tissue damage containing large numbers of apoptotic and necrotic cells (Jackson, 1969; Shupp et al., 2010). Using acridine orange (Abrams et al., 1993), we found that thermal injury led to an increase in apoptotic cells compared with uninjured larvae at 6 hpb (Figure S2A). To address whether the presence of damaged tissue contributes to leukocyte recruitment, we excised the burn tissue at 24 hpb and quantified leukocyte recruitment at 48 hpb (Figure 3A). Larvae that received double transection wounds (first at 0 h and again at 24 h) exhibited an increase in neutrophils and macrophages at the wound at 48 hpw compared with a single transection wound at 0 h (Figures 3B and 3C). In contrast, excision of the burn tissue at 24 hpb trended toward a reduction in neutrophils and a significant reduction in macrophages at the wound, compared with a non-excised burn (Figures 3B and 3C). These findings indicate that the damaged tissue in burn wounds serves as a key signal source for sustained leukocyte recruitment and that removing the damaged tissue may reduce tissue inflammation.

To address the question of what signals from the damaged tissue contribute to the sustained inflammatory response, we considered soluble chemotactic signals released by damaged tissue, such as adenosine triphosphate (ATP) and hydrogen peroxide (H_2O_2), that regulate early leukocyte recruitment to a wound (Harada et al., 2018; Niethammer et al., 2009; de Oliveira et al., 2014; Yoo et al., 2011). ATP is a well-described damage signal with pleiotropic downstream inflammatory effects (Cauwels et al., 2014). To test the impact of ATP signaling on leukocyte recruitment to the thermal injury, larval caudal fins were burned in the presence of apyrase (Figure 3D), an ATP-diphosphohydrolase that leads to the degradation of ATP (Gault et al., 2014). Apyrase treatment with thermal injury decreased the number of neutrophils at 6 hpb (Figure 3E). However, macrophage recruitment was unaffected by apyrase treatment during these timepoints, suggesting that macrophage recruitment is not dependent on ATP during early time points (Figure 3F).

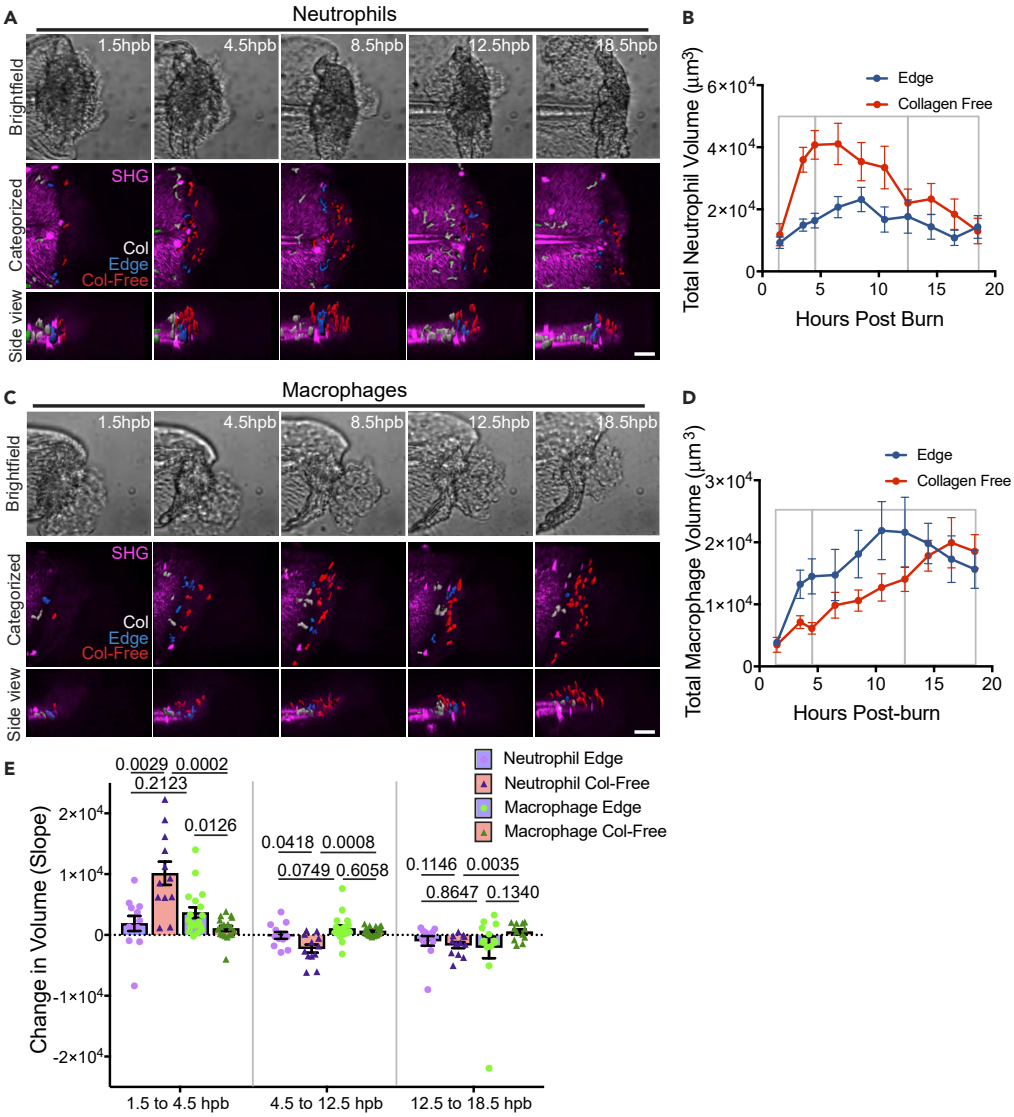

Figure 2. Macrophages and Neutrophils Differ in Their Residency in the Collagen-Free Region of the Burn Wound

(A and C) Images generated from multiphoton microscopy images of (A) neutrophils or (C) macrophages and collagen fibers during the first 18.5 hpb in a live larva. Top row: Brightfield images show overall tissue changes. Middle row: Surface rendered leukocytes (Imaris) were categorized by location: in the collagen zone (white), at the edge of the collagen (blue) or in the collagen-free zone (red), with SHG fibers in magenta. Bottom row: Side view of the surface rendered, 3D reconstruction demonstrating the 3D nature of these zones. Scale bars, 50 µm.

(B) Total volume of the surface rendered, categorized neutrophils in edge and collagen-free zone over time. Gray boxes indicate time windows used for graph in (E) Symbols indicate arithmetic mean with SE.

(D) Total volume of the surface rendered, categorized macrophages in each zone over time. Gray boxes indicate time windows used for graph in (E) Symbols indicate arithmetic mean with SE.

(E) Comparison of the change (slope) in total volume of neutrophils (magenta) and macrophages (green) for each larva in either edge (blue columns with round symbols) or collagen-free (peach columns with triangle symbols) wound zones in three different time windows, identified by the gray boxes in (B) and (D). Symbols represent individual larva; columns are arithmetic mean with SE. Additional statistical values in Table S1. See also Figure S1 and Video S2.

Hydrogen peroxide is also an important leukocyte chemoattractant *in vivo* (Chang et al., 2013; Klyubin et al., 1996; Niethammer et al., 2009; Yoo et al., 2011). Blocking H_2O_2 release reduces the number of macrophages and neutrophils at a tail transection wound in zebrafish (Niethammer et al., 2009; de Oliveira et al., 2014; Tauzin et al., 2014; Yoo et al., 2011). To determine the role of H_2O_2 following thermal injury, larvae were incubated with diphenyleneiodonium chloride (DPI), which prevents H_2O_2 production during

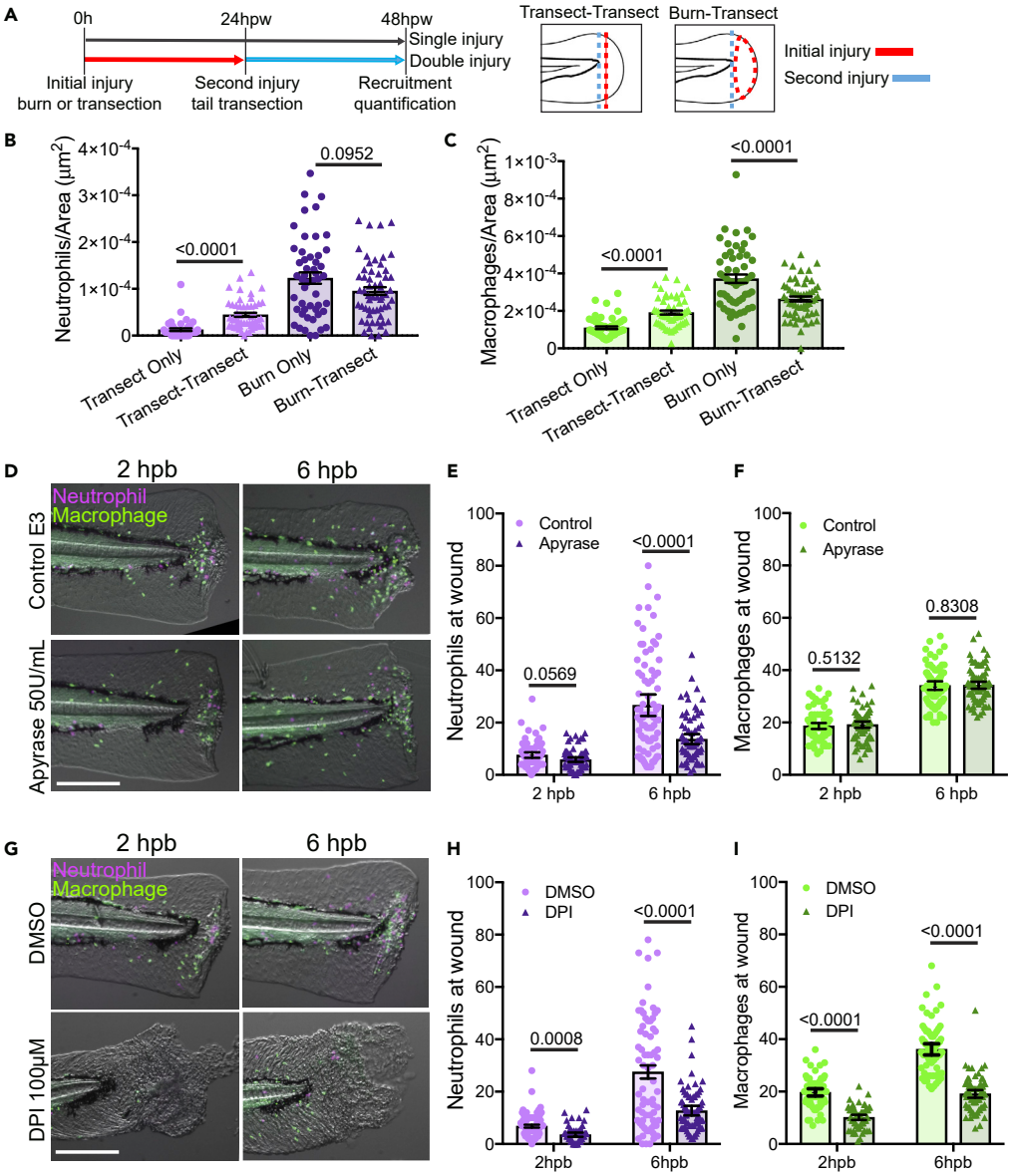

Figure 3. Neutrophil Recruitment to Thermal Injury Depends on Both ATP and ROS, whereas Macrophage Recruitment Depends Only on ROS

(A) Schematic illustrating the experiment design. Burn or tail transection was performed on 3-dpf larvae. After 24 h of the initial insult, burn tissue was excised or a second transection was performed.

(B) Neutrophil recruitment quantified 24 h after the second insult (48 h after initial injury). Neutrophil numbers were normalized to fin area for each larva. Symbols indicate individual larvae.

(C) Macrophage recruitment quantified 24 h after the second insult (48 h after initial injury). Macrophage numbers were normalized to fin area for each larva. Symbols indicate individual larvae.

(D) Representative images of 3-dpf larvae burned in the presence of apyrase then macrophage (green) and neutrophil (magenta) recruitment were quantified at 2 and 6 hpb. Scale bars, 200 μm.

(E and F) Recruitment of (E) neutrophils and (F) macrophages to the burn wound with apyrase treatment. Symbols indicate individual larvae.

(G) Representative images of 3-dpf larvae burned in the presence of DPI (1 h pre- and post-burn treatment) and macrophage (green) and neutrophil (magenta) recruitment was quantified at 2 and 6 hpb. Scale bars, 200 μm.

(H and I) Recruitment of neutrophils and macrophages, (H) and (I) respectively, to the burn wound with DPI treatment. Symbols indicate individual larvae. For (B), (C), (E), (F), (H), and (I) columns are mean with SE. Additional statistical values in Table S1. See also Figure S2.

wounding (Figure 3G) (Yoo et al., 2011). Consistent with the previous observations of leukocyte recruitment to tail transection (Niethammer et al., 2009; de Oliveira et al., 2014; Yoo et al., 2011), H_2O_2 production inhibition with DPI impaired both neutrophil and macrophage recruitment to a burn wound at 2 and 6 hpb (Figures 3H and 3I). Of note, DPI treatment had some direct damaging effects on fin morphology compared with control vehicle but, despite this damage, leukocyte recruitment was still impaired. These results suggest that, although some common cues, such as H_2O_2, mediate both neutrophil and macrophage recruitment, distinct cues, like ATP, may differentially mediate leukocyte responses to thermal injury.

Neutrophils Are Present in Human Burns and Impair Zebrafish Burn Wound Healing

To ascertain whether a neutrophil response observed in zebrafish was present in human burn wounds we examined the RNA expression of several sets of genes in human burn tissue samples. Utilizing previously published expression data from biopsies of burn patients with both partial and full thickness burns (Karim et al., 2019b), we re-examined these expression data to determine the levels of neutrophil-related genes. In both deep partial-thickness (DPT) and full-thickness (FT) burns, neutrophil markers increased compared with the control (Figure 4A, Data S1), establishing that neutrophil response to thermal injury in humans is increased, similar to that observed in zebrafish larvae. This is consistent with published histology showing neutrophil infiltration in burns. Furthermore, the timing of recruitment seen in our work follows similar trends as seen by others in different burn models (Van De Groot et al., 2009; Lateef et al., 2019). We next sought to determine whether the presence of neutrophils impacts burn wound resolution. To accomplish this, we assessed burn wound regrowth in *Tg*(*mpx:Rac2*^{D57N}-*mCherry*) transgenic larvae. This dominant negative Rac2 prevents neutrophil migration out of the caudal hematopoietic tissue and subsequent recruitment to a wound (Deng et al., 2011). Tissue regrowth at 72 h after burn injury was significantly improved in Rac2^{D57N} larvae as compared with wild-type (Figure 4B). This suggests that the presence of neutrophils is inhibitory to burn wound healing in this model, consistent with studies in mouse models (Dovi et al., 2003).

Neutrophil, but Not Macrophage, Recruitment Depends on IL-6

Owing to the importance of neutrophil infiltration into burn tissue, we next aimed to investigate signaling pathways that could influence this behavior. Our recent studies implicate IL-6 signaling in neutrophil motility in 3D *in vitro* (Hind et al., 2018). Furthermore, IL-6 is upregulated in burn patient serum and circulating levels of IL-6 correlate with reduced patient survival (Gauglitz et al., 2008; Yeh et al., 1999). We identified a significant increase in expression of IL-6-related pathway genes in full thickness burns compared with control (Figure 4C, Data S1). Although IL-6 blockade is used to treat chronic inflammatory disease (Noack and Miossec, 2017), the specific role of IL-6 signaling on inflammation in response to burn injury remains unclear. To investigate the role of IL-6 signaling in response to thermal injury in zebrafish, we characterized an IL-6 receptor (*il-6r*) mutant zebrafish line (Sa42709; ZIRC). Protein sequence alignment predicts several key conserved domains between human and zebrafish *il-6r* (Figure S3A; ENSEMBL: ENSDART00000186042.1). These conserved domains include the IL-6 binding domain, signal transduction domains and IL-6 receptor family cysteine residues (Yawata et al., 1993). The *il-6r* mutant zebrafish line (*il-6r* $^{-/-}$) is predicted to have a premature stop codon within exon 1 (L42 > Stop; Figure S3A) and, indeed, RT-qPCR showed that mRNA transcript abundance was decreased in *il-6r*$^{-/-}$ larvae, suggesting that the mutation affects mRNA stability (Figure S3B). *il-6r*$^{-/-}$ zebrafish were outcrossed into the *Tg(mpeg1:H2B-GFP/lyzc:H2B-mCherry)* line, permitting quantification of leukocyte responses to thermal injury in the absence of the *il-6r* (Figure 4D). Neutrophil recruitment to the burn wound was significantly decreased in the *il-6r* $^{-/-}$ larvae compared with both *il-6r*$^{+/+}$ and *il-6r*$^{+/-}$ matched siblings at 2, 6, and 24 hpb (Figure 4E). Additionally, heterozygous *il-6r*$^{+/-}$ larvae exhibited an intermediate decrease in neutrophil recruitment compared with *il-6r*$^{+/+}$ siblings at 6 hpb (Figure 4E), suggesting that the concentration of the IL-6R regulates neutrophil recruitment to burn injury. In contrast, macrophage recruitment to burn injury was generally unaffected by loss of *il-6r* (Figure 4F). At 6 h after burn *il-6* expression exhibited increased levels in the tail compared with control, although this trend was not statistically significant (Figure S3C). However, we also observed reduced recruitment of neutrophils to a tail transection wound in IL-6R-deficient larvae (Figure S3D), supporting previous reports that IL-6 also plays a role in other types of injuries (Biffl et al., 1996; Tompkins, 2015). Depletion of IL-6R also did not affect the total number of either neutrophils or macrophages in larval zebrafish (Figure S3E), indicating that lower neutrophil recruitment to the thermal injury is not due to developmental defects in leukocyte production.

To confirm specificity of the *il-6r* mutation, zebrafish *il-6r* mRNA was amplified from wild-type cDNA to rescue the mutant line. Two alternatively spliced isoforms of *il-6r* were identified (Figure S3A, GenBank:

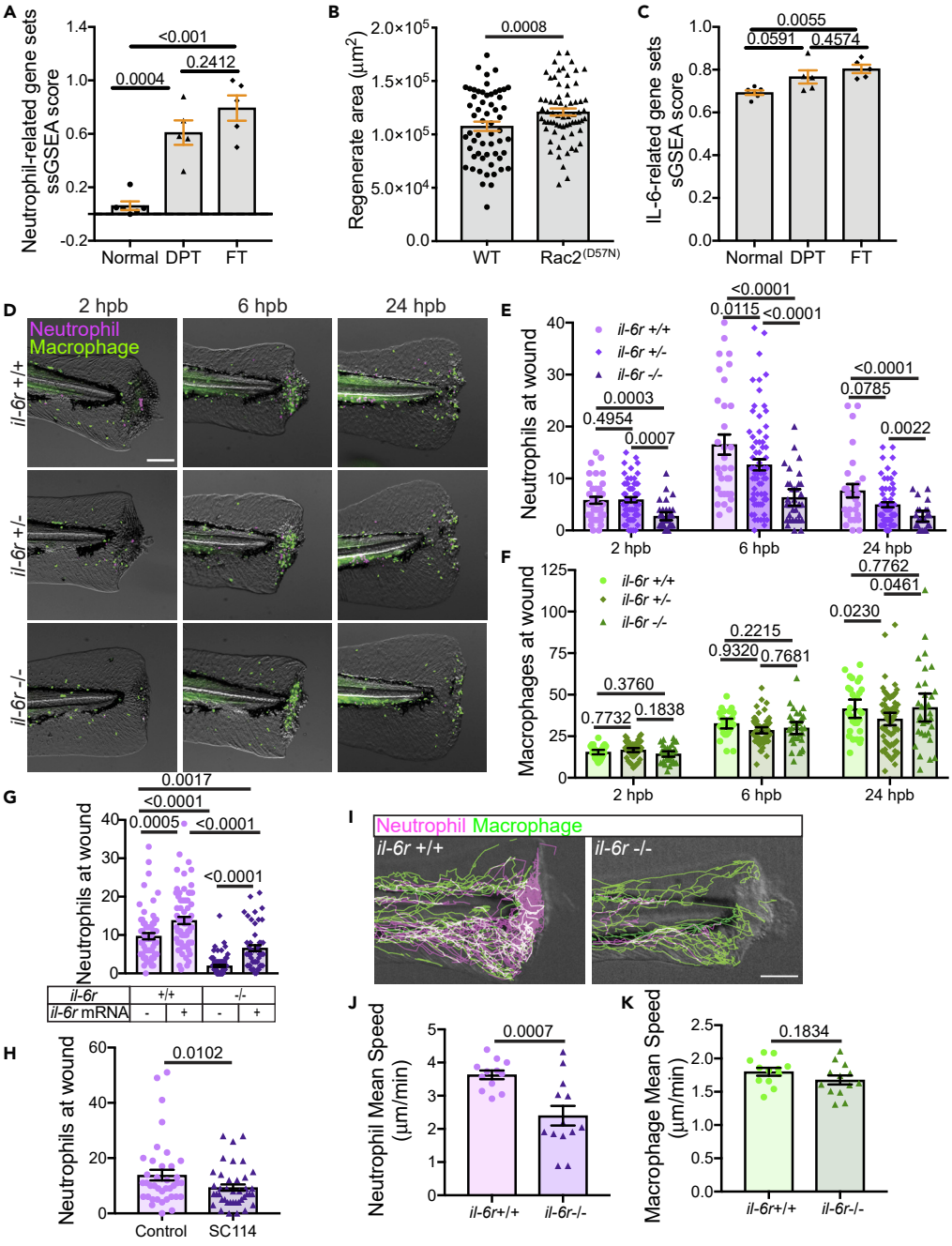

Figure 4. Neutrophil Recruitment to a Burn Wound Is IL-6 Dependent

(A) RNA expression of neutrophil-related genes (source: geneontology.org) of normal, deep partial-thickness (DPT) and full-thickness (FT) burn samples from human biopsies. Symbols indicate patient biopsies.

(B) Fin regeneration area at 72 hpb in wild-type and Rac2^{D57N} larvae. Symbols indicate individual larvae.

(C) Expression of IL-6-related pathway genes (Source: Biocarta) in human burn patient biopsies. Data for (A) and (C) from single sample Gene set Enrichment Analysis (ssGSEA). Symbols indicate patient biopsies.

(D) Representative images showing neutrophils (magenta) and macrophages (green) in 3-dpf larvae, carrying WT (+/+), heterozygous (+/−), or mutant alleles (−/−) for *il-6r*, at 2, 6, and 24 h following thermal injury. Scale bar, 200 µm.

(E) Number of neutrophils present in the burn wound in the different *il-6r* allele backgrounds. Symbols indicate individual larvae.

(F) Number of macrophages present in the burn wound in the different *il-6r* allele backgrounds. Symbols indicate individual larvae.

Figure 4. *Continued*

(G) Quantification of neutrophil recruitment to the burn wound at 6 hpb in larvae with and without injection of *il-6r* mRNA (isoform #1). Symbols indicate individual larvae.

(H) Quantification of neutrophil number at 6 hpb when IL-6R binding to gp130 was inhibited with SC144 treatment. Symbols indicate individual larvae.

(I) Representative images of cumulative automated tracks of neutrophils (magenta) and macrophages (green) overlayed on DIC images of *il-6r*$^{+/+}$ or *il-6r*$^{-/-}$ thermally injured caudal fins at 6 hpb. Scale bar, 100 μm.

(J) Quantification of mean neutrophil speed in *il-6r*$^{+/+}$ or *il-6r* $^{-/-}$ over 6 h following thermal injury. Symbols indicate individual larvae.

(K) Quantification of mean macrophage speed in *il-6r* $^{+/+}$ or *il-6r* $^{-/-}$ over 6 h following thermal injury. Symbols indicate individual larvae. For (A)–(C), (E)–(H), (J), and (K) columns are arithmetic mean with SE. Additional statistical values in Table S1. See also Figure S3 and Videos S3 and S4.

MW067024; MW067025). Isoform #2 is generally similar to the zebrafish *il-6r* consensus sequence, whereas isoform #1 lacks exon 8, generating an early stop codon (Figure S3A). Consensus Constrained TOPology prediction (CCTOP) and Phobius *in silico* analysis (Dobson et al., 2015; Käll et al., 2004) predicted that isoform #1 lacks the transmembrane and cytoplasmic domain (Figure S3A), suggesting this is a soluble isoform of IL-6R. This is consistent with previously described soluble human isoforms of IL-6R lacking the transmembrane domain due to alternative splicing of the last exon (Baran et al., 2018; Heaney and Golde, 1996; Horiuchi et al., 1994). Importantly, the human soluble form of IL-6R is still capable of binding IL-6 and signaling through the coreceptor, gp130 (Hurst et al., 2001; Jones et al., 2001). We found that the reduction in neutrophil recruitment to thermal injury in *il-6r* $^{-/-}$ larvae was partially rescued by injection of mRNA of the identified soluble form of the *il-6r* (Isoform #1) (Figure 4G). Furthermore, *il-6r* $^{+/+}$ larvae injected with the same *il-6r* isoform mRNA exhibited an increase in neutrophil recruitment to a burn, further suggesting that *il-6r* works in a dose-dependent manner for neutrophil recruitment following thermal injury (Figure 4G). Additionally, neutrophil recruitment was decreased during a thermal injury response when the binding of the IL-6R to its co-receptor gp130 was inhibited using the small molecule SC144 (Figure 4H) (Xu et al., 2013). Together, these findings support a critical role for IL-6 signaling in neutrophil recruitment to thermal damage. These findings are consistent with previous work reporting that IL-6 is important for neutrophil migration toward IL-8, fMLP, and LPS-induced pulmonary inflammation and infection (Fielding et al., 2008; Hind et al., 2018; Wright et al., 2014; Yan et al., 2013).

To determine the impact of the IL-6 receptor on leukocyte migration, we used the *il-6r*$^{-/-}$*Tg(mpeg1:H2B-GFP/lyzc:H2B-mCherry)* line described above and tracked leukocyte movement during early burn responses. In mutant larvae, neutrophils, but not macrophages, showed a striking migratory defect compared with WT larvae (Figures 4I and Videos S3 and S4). Quantification of migratory parameters showed that the mean neutrophil speed was significantly reduced in *il-6r*$^{-/-}$ compared with *il-6r*$^{+/+}$ larvae (Figure 4J), whereas the macrophage speed was unaffected (Figure 4K). These results suggest that neutrophil, but not macrophage, motility in response to burn wounds is dependent on the IL-6 receptor.

The IL-6 Receptor Is Not Necessary for Neutrophil Recruitment to *Pseudomonas aeruginosa*-Infected Burn Wounds

To further investigate the role of *il-6r* during thermal injury, we imaged the response of leukocytes to infected wounds. *Pseudomonas aeruginosa* is one of the most common pathogens found in burn patients and leads to higher morbidity and mortality (Estahbanati et al., 2002). Therefore, wound responses were investigated in the presence of *P. aeruginosa* (PA14 strain) infection after thermal injury (Figures 5A, 5B,and S4A). We found that tissue re-growth was impaired with *P. aeruginosa*-infected wounds (Figure 5C). Although *P. aeruginosa* infection was mostly cleared by 96 hbp (Figure S4A), infection of burn wounds resulted in an increased and sustained recruitment of both neutrophils and macrophages at the injured site from 2 to 96 hpb (Figures S4B and S4C). In both control and IL-6 receptor-depleted larvae neutrophil recruitment was increased with infection compared with uninfected wounds at 6 and 24 hpb (Figure S4D). However, the fold change in neutrophil recruitment to *P. aeruginosa*-infected wounds in *il-6r*$^{-/-}$ mutant larvae was not decreased compared with the infected *il-6r*$^{+/+}$ at 6 hpb. This is in contrast to the dramatic decrease in neutrophil recruitment observed in uninfected *il-6r*$^{-/-}$ compared with wild-type larvae (Figures 5D and S4D). Additionally, the fold change in neutrophil recruitment in *il-6r*$^{-/-}$ mutant larvae was greater in the presence of *P. aeruginosa* infection at both 6 and 24 hpb. Together, these data suggest that *il-6r* is not required for neutrophil recruitment to infected wounds. Macrophage recruitment to infected burn wounds was slightly decreased in *il-6r*$^{-/-}$ larvae at 6 hpb, but there was no difference in recruitment observed at 24

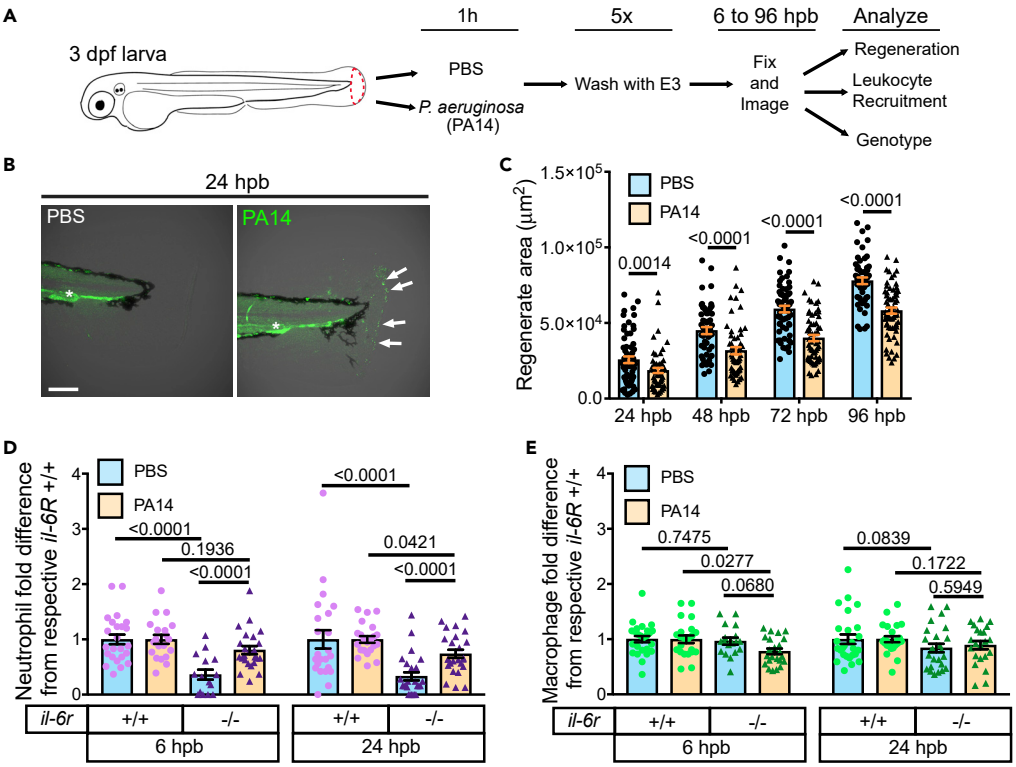

Figure 5. IL-6 Receptor Is Not Required for Neutrophil Recruitment to Infected Burn Wounds

(A) Diagram describing the protocol for infection of burn wounds with *P. aeruginosa* (PA14 strain). Larvae, 3 dpf, were burned, followed immediately by a 1-h exposure to bacteria or PBS. Fin regeneration and leukocyte recruitment were quantified and larvae were subsequently genotyped.

(B) Fluorescent micrographs showing the presence of PA14 bacteria in thermally injured caudal fin at 24 hpb. Arrows indicate bacteria in infected tails; asterisk denotes non-specific background fluorescence. Scale bar, 200 μm.

(C) Area of tissue regrowth in burned caudal fins with and without PA14 infection, measured as the fin tissue caudal to the posterior end of the notochord. Symbols indicate individual larvae.

(D) Comparison of neutrophil recruitment to the burn wound site with bacteria (PA14 - beige columns) or without bacteria (PBS - blue columns) in *il-6r* $^{+/+}$ or *il-6r* $^{-/-}$ larvae depicted as the fold change in neutrophil number relative to the mean of the corresponding wild-type. Symbols indicate individual larvae.

(E) Comparison of macrophage recruitment to the burn wound site, with bacteria (PA14, beige columns) or without bacteria (PBS, blue columns) in *il-6r* $^{+/+}$ or *il-6r* $^{-/-}$ larvae, depicted as the fold change in macrophage number relative to the mean of the corresponding wild-type. Symbols indicate individual larvae. Graphs with neutrophil counts and heterozygote data are presented in Figure S4. For (C)–(E) columns are arithmetic mean with SE. Additional statistical values in Table S1. See also Figure S4.

hpb (Figures 5E and S4E). In all, these findings suggest that the IL-6 receptor is required for neutrophil recruitment to tissue damage but not to infected wounds.

DISCUSSION

Thermal injury induces complex tissue damage that has significant morbidity and mortality worldwide. Both damage and microbial cues recruit innate phagocytes, and the balance of this inflammation can determine clinical outcome (Church et al., 2006; Ipaktchi et al., 2006). We identified IL-6 as a key signal that controls neutrophil responses to sterile thermal injury but is not necessary for neutrophil recruitment to wounds infected with *P. aeruginosa*, a common pathogen found in human burn injuries (Gonzalez et al., 2018). Our findings highlight context-dependent signals that differentially regulate neutrophil and macrophage responses that impact tissue repair.

Leukocyte behavior is regulated by the tissue microenvironment; however, the ability to image leukocyte movement within interstitial tissues with high resolution has limited the field. Few models allow for the

direct visualization of leukocyte-ECM dynamics in real time. Zebrafish caudal fins contain radially organized collagen fibers (LeBert et al., 2015), which are lost after burn injury (LeBert et al., 2018; Miskolci et al., 2019), similar to the loss of ECM organization observed in murine skin after thermal injury (Lateef et al., 2019). Here we show distinct motile behaviors of neutrophils and macrophages in interstitial tissues after thermal injury, with striking differences in neutrophil and macrophage recruitment into the "collagen-free" zone. Macrophages exhibit pausing and slower migration at the interface between collagen-containing and the wound-induced collagen-free zones. By contrast, neutrophils exhibit rapid, swarming migration into the collagen-free zone in a fashion similar to other migratory amoeboid cells *in vivo* (Lämmermann et al., 2013). For example, neutrophils move into other collagen-free zones including the luminal parts of the intestine and vasculature (Massena et al., 2010; Sumagin et al., 2014). Our previous studies demonstrated that macrophages exhibit a mesenchymal-like mode of migration in interstitial tissues in zebrafish that requires proteolytic activity, whereas neutrophils demonstrate amoeboid migration that is not protease sensitive (Barros-Becker et al., 2017). Taken together, these findings show that, in contrast to macrophages, neutrophils are less sensitive to changing collagen ECM structure and can rapidly migrate in areas devoid of organized collagen *in vivo*.

Pro-inflammatory signals, such as DAMPs, are released from damaged tissues and mediate leukocyte recruitment in response to apoptotic and necrotic cells (Gravante et al, 2006a, 2006b; Shupp et al., 2010; Singer et al., 2008). Damage signals that modulate early leukocyte recruitment include adenosine triphosphate (ATP) and reactive oxygen species (ROS). ATP released during injuries rapidly induces leukocyte migration (Boucher et al., 2010; de Oliveira et al., 2014). Both neutrophils and macrophages strongly respond to ATP gradients (Chen et al., 2006; Kronlage et al., 2010; Wang and Chen, 2018; Wang and Kubes, 2016) and this effect can be reduced by treatment with apyrase (Kronlage et al., 2010; de Oliveira et al., 2014). Interestingly, we found that neutrophil, but not macrophage, recruitment to burn injury was reduced by apyrase, suggesting that the cues mediating the recruitment of neutrophils and macrophages to thermal injury are separable. It is not clear if the neutrophil effect was a direct result of ATP reduction or indirect through effects of ATP on other signaling pathways, including ROS-mediated production of MIP-2 in macrophages, which then could induce neutrophil recruitment, as documented in mice (Kawamura et al., 2012). In contrast to ATP, we found that ROS signaling was important for both early and late neutrophil and macrophage recruitment to thermal injury. ROS is widely recognized as an important neutrophil chemoattractant to damage, resulting in recruitment early after tail transection (Niethammer et al., 2009; Yoo et al., 2011). Although it is not clear if these effects are direct, neutrophils can sense H_2O_2 through the oxidation of downstream signaling components, like Lyn, as an early signaling mechanism (Yoo et al., 2011). Alternatively, H_2O_2 could be acting through general tissue activation of the NF-kB/AP1 signaling pathway and contribute to later recruitment via the production of other pro-inflammatory mediators, such as IL-8 and IL-6 (Chang et al., 2013; de Oliveira et al., 2014; Wittmann et al., 2012). Interestingly, removal of the damaged tissue after burn reduces recruitment of both neutrophils and macrophages to the wound. Early excision of burns in humans with a large total body surface area injury decreases mortality, an effect thought to be due to the reduction of the inflammatory burden of the necrotic tissue (Ong et al., 2006). Further study is needed to determine if removal of the damaged tissue reduces DAMP-mediated recruitment or whether this removal is impacting other wound-specific signals.

Our results, along with previous reports, show that IL-6 is upregulated after burn injury in human patients and in murine burn models (Abdullahi et al., 2014; Drost et al., 1993; Hager et al., 2018). We detected a similar trend in *il-6* expression through our zebrafish RT-qPCR, although these results are not statistically significant. This cytokine regulates neutrophil migration toward IL-8 and fMLP, thereby impacting LPS-induced pulmonary inflammation, infection, and peritoneal acute inflammation (Fielding et al., 2008; Hind et al., 2018; Wright et al., 2014; Yan et al., 2013). Our findings show that depletion of the IL-6R in zebrafish decreases neutrophil recruitment to burn injury. IL-6 expression can be induced by several factors, including LTB4, ATP, INF-γ, and NF-kB activation (Faggioli et al., 1997; Ihara et al., 2005; Tanaka et al., 2014). This leads to the activation of STAT3 and several pro-inflammatory genes, including chemokine receptors such as the IL-8 receptor, CXCR2 (Nguyen-Jackson et al., 2010). IL-6 expression also generates a positive feedback loop, further activating IL-6 signaling pathways (Hendrayani et al., 2016; Lee et al., 2012). Our data suggest that IL-6 signaling could be involved in initiating and maintaining a primed state in neutrophils after burn injury, which is impaired in the *il-6r*$^{-/-}$ mutants, leaving neutrophils less sensitive to specific external inflammatory cues. Bacterial infection of the burn injury by *P. aeruginosa* shows that neutrophils from *il-6r* mutants are capable of migrating in great numbers to the damaged area in the presence

of microbial cues, albeit to a slightly lesser degree than that of the infected wild-type larvae. This suggests that neutrophil deficiency after loss of IL-6R is not related to impaired cell movement. It is possible that IL-6 acts as a neutrophil motility priming factor that mediates recruitment to sterile damage cues. Interestingly, loss of IL-6R has no noticeable effect on macrophage recruitment to burn injury. IL-6 signaling has been shown to regulate macrophage polarization, favoring an M2 state, by alternatively activating macrophages (Chen et al., 2018; Fernando et al., 2014; Mauer et al., 2014). Therefore, although IL-6 signaling does not affect macrophage recruitment to burn injury in zebrafish larvae, more work is necessary to explore the impact of IL-6 on macrophage polarization within burn wounds.

Both microbes and tissue damage signaling recruit neutrophils to the site of insult. A recent report by Huang and Niethammer (2018) showed that neutrophils require tissue damage signaling to respond to microbial cues in the otic vesicle of zebrafish. Here, we show that IL-6 is a tissue damage cue that mediates neutrophil recruitment to sterile thermal injury. The presence of bacteria can override the neutrophil recruitment inhibition in *il-6r* mutants, suggesting that even when specific tissue damage cues are blocked, neutrophils can still respond to microbial cues. It is possible that the hierarchy of recruitment signaling is context dependent such that the extensive disruption of the matrix architecture that occurs with thermal injury may induce distinct tissue damage cues that are separable from microbial cues. This distinction potentially provides a therapeutic target to block damaging neutrophil inflammation in burns with IL-6 blockade, while still permitting neutrophil responses to pathogenic infection.

In conclusion, zebrafish provide a new model in which to study the innate immune response during early burn injury. Tissue morphology changes and loss of collagen fibers affect macrophage, but not neutrophil, recruitment to the wound area. We demonstrate that IL-6 signaling is critical for neutrophil motility and recruitment during early burn wound response but not in the presence of pathogenic microbes. Further work will be needed to determine the complete role of IL-6 signaling and its potential for therapeutic benefit in burn patients. This work provides a framework for the identification of pathways that limit damaging neutrophil inflammation in sterile injuries while not impacting necessary neutrophil responses to microbial injury.

Limitations of the Study

This study shows the complex environment under which neutrophils and macrophages need to respond during early burn injuries. The specific abundance of different signals, soluble and insoluble, can affect each cell type individually, influencing their response. However, further studies are needed to define the specifics of the relationship between changes in the matrix architecture of a burn injury and neutrophil and macrophage migration. Moreover, further studies are needed to elucidate the cellular origin of *il-6* as well as the molecular downstream effects of *il-6* on neutrophil activation, especially during a sterile burn injury.

Resource Availability

Lead Contact

Further information and requests for data, resources, and reagents should be directed to, and will be fulfilled, by the Lead Contact, Anna Huttenlocher (huttenlocher@wisc.edu).

Materials Availability

Plasmids and zebrafish lines generated in this study are available from the lead contact upon request.

Data and Code Availability

Original/source data for all figures published in this study are available from the lead contact upon request. The sequences generated in this study are available at GenBank (Accession number MW067024 for il-6r isoform #1 and MW067025 for *il-6r* isoform #2). This study did not generate any new code.

METHODS

All methods can be found in the accompanying Transparent Methods supplemental file.

SUPPLEMENTAL INFORMATION

Supplemental Information can be found online at https://doi.org/10.1016/j.isci.2020.101699.

ACKNOWLEDGMENTS

We would like to thank all Huttenlocher lab members for useful discussion and input. We would like to thank Drs. Veronika Miskolci and Adam Horn for critical reading of the manuscript. We would like to thank Jens Eickhoff for advice on statistical analysis. This work was supported by NIH R35 GM1 18027 (A.H.).

AUTHOR CONTRIBUTIONS

Conceptualization, F.B.-B., J.M.S., and A.H. Methodology, F.B.-B. and J.M.S. Investigation, F.B.-B., J.M.S., R.B., J.C., and J.R. Formal analysis, F.B.-B., J.M.S., R.B., and A.K. Statistical analysis, J.M.S. Human expression data analysis, A.K. Visualization, F.B.-B. and J.M.S. Writing, F.B.-B., J.M.S., and A.H., with input of all other authors. Resources, A.H. and K.W.E. Funding acquisition, A.H.

DECLARATION OF INTERESTS

The authors declare no competing interests.

Received: July 9, 2020
Revised: September 17, 2020
Accepted: October 14, 2020
Published: November 20, 2020

REFERENCES

Abdullahi, A., Amini-Nik, S., and Jeschke, M.G. (2014). Animal models in burn research. Cell. Mol. Life Sci. *71*, 3241–3255.

Abrams, J.M., White, K., Fessler, L.I., and Steller, H. (1993). Programmed cell death during Drosophila embryogenesis. Development *117*, 29–43.

Baran, P., Hansen, S., Waetzig, G.H., Akbarzadeh, M., Lamertz, L., Huber, H.J., Ahmadian, M.R., Moll, J.M., and Scheller, J. (2018). The balance of interleukin (IL)-6, IL-6·soluble IL-6 receptor (sIL-6R), and IL-6·sIL-6R·sgp130 complexes allows simultaneous classic and trans-signaling. J. Biol. Chem. *293*, 6762–6775.

Barros-Becker, F., Lam, P., Fisher, R., and Huttenlocher, A. (2017). Live imaging reveals distinct modes of neutrophil and macrophage migration within interstitial tissues. J. Cell Sci. *130*, 3801–3808.

Bayliss, J., Delarosa, S., Wu, J., Peterson, J.R., Eboda, O.N., Su, G.L., Hemmila, M., Krebsbach, P.H., Cederna, P.S., Wang, S.C., et al. (2014). Adenosine triphosphate hydrolysis reduces neutrophil infiltration and necrosis in partial-thickness scald burns in mice. J. Burn Care Res. *35*, 54–61.

Biffl, W.L., Moore, E.E., Moore, F.A., and Peterson, V.M. (1996). Interleukin-6 in the injured patient: marker of injury or mediator of inflammation? Ann. Surg. *224*, 647–664.

Boucher, I., Rich, C., Lee, A., Marcincin, M., and Trinkaus-Randall, V. (2010). The P2Y2 receptor mediates the epithelial injury response and cell migration. Am. J. Physiol. Cell Physiol. *299*, C411–C421.

Cauwels, A., Rogge, E., Vandendriessche, B., Shiva, S., and Brouckaert, P. (2014). Extracellular ATP drives systemic inflammation, tissue damage and mortality. Cell Death Dis. *5*, e1102.

Chang, S., Linderholm, A., Franzi, L., Kenyon, N., Grasberger, H., and Harper, R. (2013). Dual oxidase regulates neutrophil recruitment in allergic airways. Free Radic. Biol. Med. *65*, 38–46.

Chen, Y., Corriden, R., Inoue, Y., Yip, L., Hashiguchi, N., Zinkernagel, A., Nizet, V., Insel, P.A., and Junger, W.G. (2006). ATP release guides neutrophil chemotaxis via P2Y2 and A3 receptors. Science *314*, 1792–1795.

Chen, L., Wang, S., Wang, Y., Zhang, W., Ma, K., Hu, C., Zhu, H., Liang, S., Liu, M., and Xu, N. (2018). IL-6 influences the polarization of macrophages and the formation and growth of colorectal tumor. Oncotarget *9*, 17443–17454.

Church, D., Elsayed, S., Reid, O., Winston, B., and Lindsay, R. (2006). Burn wound infections. Clin. Microbiol. Rev. *19*, 403–434.

von Dassow, G., Verbrugghe, K.J.C., Miller, A.L., Sider, J.R., and Bement, W.M. (2009). Action at a distance during cytokinesis. J. Cell Biol. *187*, 831–845.

Van De Groot, F., Krijnen, P.A.J., Begieneman, M.P.V., Ulrich, M.M.W., Middelkoop, E., and Niessen, H.W.M. (2009). Acute inflammation is persistent locally in burn wounds: a pivotal role for complement and C-reactive protein. J. Burn Care Res. *30*, 274–280.

Deng, Q., Yoo, S.K., Cavnar, P.J., Green, J.M., and Huttenlocher, A. (2011). Dual roles for Rac2 in neutrophil motility and active retention in zebrafish hematopoietic tissue. Dev. Cell *21*, 735–745.

Dobson, L., Reményi, I., and Tusnády, G.E. (2015). CCTOP: a Consensus Constrained TOPology prediction web server. Nucleic Acids Res. *43*, W408–W412.

Drost, A.C., Burleson, D.G., Cioffi, W.G., Jordan, B.S., Mason, A.D., and Pruitt, B.A. (1993). Plasma cytokines following thermal injury and their relationship with patient mortality, burn size, and time postburn. J. Trauma - Inj. Infect. Crit. Care *35*, 335–339.

Estahbanati, H.K., Kashani, P.P., and Ghanaatpisheh, F. (2002). Frequency of *Pseudomonas aeruginosa* serotypes in burn wound infections and their resistance to antibiotics. Burns *28*, 340–348.

Faggioli, L., Merola, M., Hiscott, J., Furia, A., Monese, R., Tovey, M., and Palmieri, M. (1997). Molecular mechanisms regulating induction of interleukin-6 gene transcription by interferon-gamma. Eur. J. Immunol. *27*, 3022–3030.

Fernando, M.R., Reyes, J.L., Iannuzzi, J., Leung, G., and McKay, D.M. (2014). The pro-inflammatory cytokine, interleukin-6, enhances the polarization of alternatively activated macrophages. PLoS One *9*, e94188.

Fielding, C.A., McLoughlin, R.M., McLeod, L., Colmont, C.S., Najdovska, M., Grail, D., Ernst, M., Jones, S.A., Topley, N., and Jenkins, B.J. (2008). IL-6 regulates neutrophil trafficking during acute inflammation via STAT3. J. Immunol. *181*, 2189–2195.

Gauglitz, G.G., Song, J., Herndon, D.N., Finnerty, C.C., Boehning, D., Barral, J.M., and Jeschke, M.G. (2008). Characterization of the inflammatory response during acute and post-acute phases after severe burn. Shock *30*, 503–507.

Gault, W.J., Enyedi, B., and Niethammer, P. (2014). Osmotic surveillance mediates rapid wound closure through nucleotide release. J. Cell Biol. *207*, 767–782.

Gonzalez, M.R., Ducret, V., Leoni, S., Fleuchot, B., Jafari, P., Raffoul, W., Applegate, L.A., Que, Y.A., and Perron, K. (2018). Transcriptome analysis of *Pseudomonas aeruginosa* cultured in human burn wound exudates. Front. Cell. Infect. Microbiol. *8*, 39.

Gravante, G., Palmieri, M.B., Esposito, G., Delogu, D., Santeusanio, G., Filingeri, V., and

Montone, A. (2006a). Apoptotic cells are present in ischemic zones of deep partial-thickness burns. J. Burn Care Res. *27*, 688–693.

Gravante, G., Filingeri, V., Delogu, D., Santeusanio, G., Palmieri, M.B., Esposito, G., Montone, A., and Sconocchia, G. (2006b). Apoptotic cell death in deep partial thickness burns by coexpression analysis of TUNEL and Fas. Surgery *139*, 854–855.

Hager, S., Foldenauer, A.C., Rennekampff, H.-O., Deisz, R., Kopp, R., Tenenhaus, M., Gernot, M., and Pallua, N. (2018). Interleukin-6 serum levels correlate with severity of burn injury but not with gender. J. Burn Care Res. *39*, 379–386.

Harada, Y., Kato, Y., Miyaji, T., Omote, H., Moriyama, Y., and Hiasa, M. (2018). Vesicular nucleotide transporter mediates ATP release and migration in neutrophils. J. Biol. Chem. *293*, 3770–3779.

Heaney, M.L., and Golde, D.W. (1996). Soluble cytokine receptors. Blood *87*, 847–857.

Hendrayani, S.-F., Al-Harbi, B., Al-Ansari, M.M., Silva, G., and Aboussekhra, A. (2016). The inflammatory/cancer-related IL-6/STAT3/NF-κB positive feedback loop includes AUF1 and maintains the active state of breast myofibroblasts. Oncotarget *7*, 41974–41985.

Hind, L.E., Ingram, P.N., Beebe, D.J., and Huttenlocher, A. (2018). Interaction with an endothelial lumen increases neutrophil lifetime and motility in response to P aeruginosa. Blood *132*, 1818–1828.

Horiuchi, S., Koyanagi, Y., Zhou, Y., Miyamoto, H., Tanaka, Y., Waki, M., Matsumoto, A., Yamamoto, M., and Yamamoto, N. (1994). Soluble interleukin-6 receptors released from T cell or granulocyte/macrophage cell lines and human peripheral blood mononuclear cells are generated through an alternative splicing mechanism. Eur. J. Immunol. *24*, 1945–1948.

Huang, C., and Niethammer, P. (2018). Tissue damage signaling is a prerequisite for protective neutrophil recruitment to microbial infection in zebrafish. Immunity *48*, 1006–1013.e6.

Hurst, S.M., Wilkinson, T.S., McLoughlin, R.M., Jones, S., Horiuchi, S., Yamamoto, N., Rose-John, S., Fuller, G.M., Topley, N., and Jones, S.A. (2001). Il-6 and its soluble receptor orchestrate a temporal switch in the pattern of leukocyte recruitment seen during acute inflammation. Immunity *14*, 705–714.

Ihara, H., Hirukawa, K., Goto, S., and Togari, A. (2005). ATP-stimulated interleukin-6 synthesis through P2Y receptors on human osteoblasts. Biochem. Biophys. Res. Commun. *326*, 329–334.

Ipaktchi, K., Mattar, A., Niederbichler, A.D., Hoesel, L.M., Vollmannshauser, S., Hemmila, M.R., Su, G.L., Remick, D.G., Wang, S.C., and Arbabi, S. (2006). Attenuating burn wound inflammatory signaling reduces systemic inflammation and acute lung injury. J. Immunol. *177*, 8065–8071.

Jackson, D.M. (1969). Second thoughts on the burn wound. J. Trauma *9*, 839–862.

Jones, S.A., Horiuchi, S., Topley, N., Yamamoto, N., and Fuller, G.M. (2001). The soluble interleukin 6 receptor: mechanisms of production and implications in disease. FASEB J. *15*, 43–58.

Käll, L., Krogh, A., and Sonnhammer, E.L.L. (2004). A combined transmembrane topology and signal peptide prediction method. J. Mol. Biol. *338*, 1027–1036.

Karim, A.S., Shaum, K., and Gibson, A.L.F. (2019a). Indeterminate-depth burn injury-exploring the uncertainty. J. Surg. Res. *245*, 183–197.

Karim, A.S., Yan, A., Ocotl, E., Bennett, D.D., Wang, Z., Kendziorski, C., and Gibson, A.L.F. (2019b). Discordance between histologic and visual assessment of tissue viability in excised burn wound tissue. Wound Repair Regen. *27*, 150–161.

Kawamura, H., Kawamura, T., Kanda, Y., Kobayashi, T., and Abo, T. (2012). Extracellular ATP-stimulated macrophages produce macrophage inflammatory protein-2 which is important for neutrophil migration. Immunology *136*, 448–458.

Klyubin, I.V., Kirpichnikova, K.M., and Gamaley, I.A. (1996). Hydrogen peroxide-induced chemotaxis of mouse peritoneal neutrophils. Eur. J. Cell Biol. *70*, 347–351.

Kronlage, M., Song, J., Sorokin, L., Isfort, K., Schwerdtle, T., Leipziger, J., Robaye, B., Conley, P.B., Kim, H.-C., Sargin, S., et al. (2010). Autocrine purinergic receptor signaling is essential for macrophage chemotaxis. Sci. Signal. *3*, ra55.

Lämmermann, T., Afonso, P.V., Angermann, B.R., Wang, J.M., Kastenmüller, W., Parent, C.A., and Germain, R.N. (2013). Neutrophil swarms require LTB4 and integrins at sites of cell death in vivo. Nature *498*, 371–375.

Lateef, Z., Stuart, G., Jones, N., Mercer, A., Fleming, S., and Wise, L. (2019). The cutaneous inflammatory response to thermal burn injury in a Murine model. Int. J. Mol. Sci. *20*, 538.

LeBert, D.C., Squirrell, J.M., Rindy, J., Broadbridge, E., Lui, Y., Zakrzewska, A., Eliceiri, K.W., Meijer, A.H., and Huttenlocher, A. (2015). Matrix metalloproteinase 9 modulates collagen matrices and wound repair. Development *142*, 2136–2146.

LeBert, D., Squirrell, J.M., Freisinger, C., Rindy, J., Golenberg, N., Frecentese, G., Gibson, A., Eliceiri, K.W., and Huttenlocher, A. (2018). Damage-induced reactive oxygen species regulate vimentin and dynamic collagen-based projections to mediate wound repair. Elife *7*, e30703.

Lee, J., Nakagiri, T., Oto, T., Harada, M., Morii, E., Shintani, Y., Inoue, M., Iwakura, Y., Miyoshi, S., Okumura, M., et al. (2012). IL-6 amplifier, NF-κB-triggered positive feedback for IL-6 signaling, in grafts is involved in allogeneic rejection responses. J. Immunol. *189*, 1928–1936.

Massena, S., Christoffersson, G., Hjertström, E., Zcharia, E., Vlodavsky, I., Ausmees, N., Rolny, C., Li, J.P., and Phillipson, M. (2010). Achemotactic gradient sequestered on endothelial heparan sulfate induces directional intraluminal crawling of neutrophils. Blood *116*, 1924–1931.

Mauer, J., Chaurasia, B., Goldau, J., Vogt, M.C., Ruud, J., Nguyen, K.D., Theurich, S., Hausen, A.C., Schmitz, J., Brönneke, H.S., et al. (2014). Signaling by IL-6 promotes alternative activation of macrophages to limit endotoxemia and obesity-associated resistance to insulin. Nat. Immunol. *15*, 423–430.

Miskolci, V., Squirrell, J., Rindy, J., Vincent, W., Sauer, J.D., Gibson, A., Eliceiri, K.W., and Huttenlocher, A. (2019). Distinct inflammatory and wound healing responses to complex caudal fin injuries of larval zebrafish. Elife *8*, e45976.

Nguyen-Jackson, H., Panopoulos, A.D., Zhang, H., Li, H.S., and Watowich, S.S. (2010). STAT3 controls the neutrophil migratory response to CXCR2 ligands by direct activation of G-CSF-induced CXCR2 expression and via modulation of CXCR2 signal transduction. Blood *115*, 3354–3363.

Niethammer, P., Grabher, C., Look, A.T., and Mitchison, T.J. (2009). A tissue-scale gradient of hydrogen peroxide mediates rapid wound detection in zebrafish. Nature *459*, 996–999.

Noack, M., and Miossec, P. (2017). Selected cytokine pathways in rheumatoid arthritis. Semin. Immunopathol. *39*, 365–383.

de Oliveira, S., López-Muñoz, A., Candel, S., Pelegrín, P., Calado, A., and Mulero, V. (2014). ATP modulates acute inflammation in vivo through dual oxidase 1-derived H2O2 production and NF-κB activation. J. Immunol. *192*, 5710–5719.

de Oliveira, S., Rosowski, E.E., and Huttenlocher, A. (2016). Neutrophil migration in infection and wound repair: going forward in reverse. Nat. Rev. Immunol. *16*, 378–391.

Ong, Y.S., Samuel, M., and Song, C. (2006). Meta-analysis of early excision of burns. Burns *32*, 145–150.

Rani, M., Nicholson, S.E., Zhang, Q., and Schwacha, M.G. (2017). Damage-associated molecular patterns (DAMPs) released after burn are associated with inflammation and monocyte activation. Burns *43*, 297–303.

Rodriguez, J.L., Miller, C.G., Garner, W.L., Till, G.O., Guerrero, P., Moore, N.P., Corridore, M., Normolle, D.P., Smith, D.J., and Remick, D.G. (1993). Correlation of the local and systemic cytokine response with clinical outcome following thermal injury. J. Trauma *34*, 684–685.

Schofield, Z.V., Woodruff, T.M., Halai, R., Wu, M.C.L., and Cooper, M.A. (2013). Neutrophils - a key component of ischemia-reperfusion injury. Shock *40*, 463–470.

Shupp, J.W., Nasabzadeh, T.J., Rosenthal, D.S., Jordan, M.H., Fidler, P., and Jeng, J.C. (2010). A review of the local pathophysiologic bases of burn wound progression. J. Burn Care Res. *31*, 849–873.

Singer, A.J., McClain, S.A., Taira, B.R., Guerriero, J.L., and Zong, W. (2008). Apoptosis and necrosis in the ischemic zone adjacent to third degree burns. Acad. Emerg. Med. *15*, 549–554.

Sumagin, R., Robin, A.Z., Nusrat, A., and Parkos, C.A. (2014). Transmigrated neutrophils in the intestinal lumen engage ICAM-1 to regulate the

epithelial barrier and neutrophil recruitment. Mucosal Immunol. *7*, 905–915.

Tanaka, T., Narazaki, M., and Kishimoto, T. (2014). IL-6 in inflammation, immunity, and disease. Cold Spring Harb. Perspect. Biol. *6*, a016295.

Tauzin, S., Starnes, T.W., Becker, F.B., Lam, P., and Huttenlocher, A. (2014). Redox and Src family kinase signaling control leukocyte wound attraction and neutrophil reverse migration. J. Cell Biol. *207*, 589–598.

Tompkins, R.G. (2015). Genomics of injury: the glue grant experience. J. Trauma Acute Care Surg. *78*, 671–686.

Valvis, S.M., Waithman, J., Wood, F.M., Fear, M.W., and Fear, V.S. (2015). The immune response to skin trauma is dependent on the etiology of injury in a mouse model of burn and excision. J. Invest. Dermatol. *135*, 2119–2128.

Wang, X., and Chen, D. (2018). Purinergic regulation of neutrophil function. Front. Immunol. *9*, 399.

Wang, J., and Kubes, P. (2016). A reservoir of mature cavity macrophages that can rapidly invade visceral organs to affect tissue repair. Cell *165*, 668–678.

Wittmann, C., Chockley, P., Singh, S.K., Pase, L., Lieschke, G.J., and Grabher, C. (2012). Hydrogen peroxide in inflammation: messenger, guide, and assassin. Adv. Hematol. *2012*, 541471.

Wright, H.L., Cross, A.L., Edwards, S.W., and Moots, R.J. (2014). Effects of IL-6 and IL-6 blockade on neutrophil function in vitro and in vivo. Rheumatology (Oxford) *53*, 1321–1331.

Xu, S., Grande, F., Garofalo, A., and Neamati, N. (2013). Discovery of a novel orally active small-molecule gp130 inhibitor for the treatment of ovarian cancer. Mol. Cancer Ther. *12*, 937–949.

Yan, B., Wei, J.-J., Yuan, Y., Sun, R., Li, D., Luo, J., Liao, S.-J., Zhou, Y.-H., Shu, Y., Wang, Q., et al. (2013). IL-6 cooperates with G-CSF to induce protumor function of neutrophils in bone marrow by enhancing STAT3 activation. J. Immunol. *190*, 5882–5893.

Yawata, H., Yasukawa, K., Natsuka, S., Murakami, M., Yamasaki, K., Hibi, M., Taga, T., and Kishimoto, T. (1993). Structure-function analysis of human IL-6 receptor: dissociation of amino acid residues required for IL-6-binding and for IL-6 signal transduction through gp130. EMBO J. *12*, 1705–1712.

Yeh, F.L., Lin, W.L., Shen, H.D., and Fang, R.H. (1999). Changes in circulating levels of interleukin 6 in burned patients. Burns *25*, 131–136.

Yoo, S.K., Starnes, T.W., Deng, Q., and Huttenlocher, A. (2011). Lyn is a redox sensor that mediates leukocyte wound attraction in vivo. Nature *480*, 109–112.

Yoo, S.K., Lam, P., Eichelberg, M.R., Zasadil, L., Bement, W.M., and Huttenlocher, A. (2012). The role of microtubules in neutrophil polarity and migration in live zebrafish. J. Cell Sci. *125*, 5702–5710.

Zhang, Q., Raoof, M., Chen, Y., Sumi, Y., Sursal, T., Junger, W., Brohi, K., Itagaki, K., and Hauser, C.J. (2010). Circulating mitochondrial DAMPs cause inflammatory responses to injury. Nature *464*, 104–107.

Dovi, J.V., He, L.-K., and DiPietro, L.A. (2003). Accelerated wound closure in neutrophil-depleted mice. J. Leukoc. Biol. *73*, 448–455.

iScience, Volume *23*

Supplemental Information

Distinct Tissue Damage and Microbial Cues Drive Neutrophil and Macrophage Recruitment to Thermal Injury

Francisco Barros-Becker, Jayne M. Squirrell, Russell Burke, Julia Chini, Julie Rindy, Aos Karim, Kevin W. Eliceiri, Angela Gibson, and Anna Huttenlocher

SUPPLEMENTAL DATA ITEMS

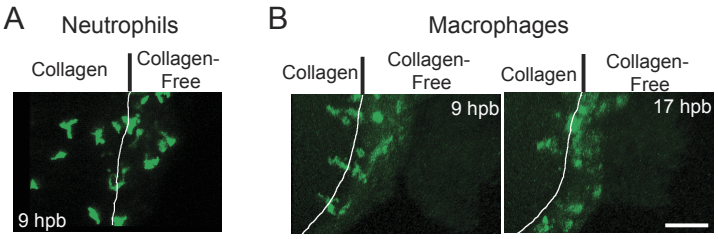

Figure S1: **Macrophages and neutrophils differ in their residency in the collagen-free region of the burn wound. Related to Figure 2.** A) Enlargement of an enface 3D reconstruction of the region around the edge (white line) of the collagen fibers, illustrating neutrophil morphology when located in either the collagen fiber region or in collagen-free tissue at 9 hpb. B) Enlargement of an enface 3D reconstruction of the region around the edge (white line) of the collagen fibers, showing macrophage morphology when located in either the collagen fiber region or in collagen-free tissue at 9 hpb and 17 hpb. Anterior is left. Scale bar = 50μm.

A

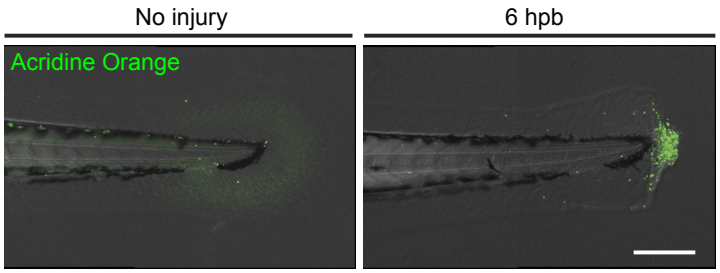

Figure S2: Burn injury shows increase apoptosis. Related to Figure 3. A) Thermal injury increased apoptosis, as shown by acridine orange staining. Representative images for two independent replicates. 3 dpf larvae were burned and stained with acridine orange at 6 hpb. Caudal fins without injury were used as control. Scale bar = 200μm.

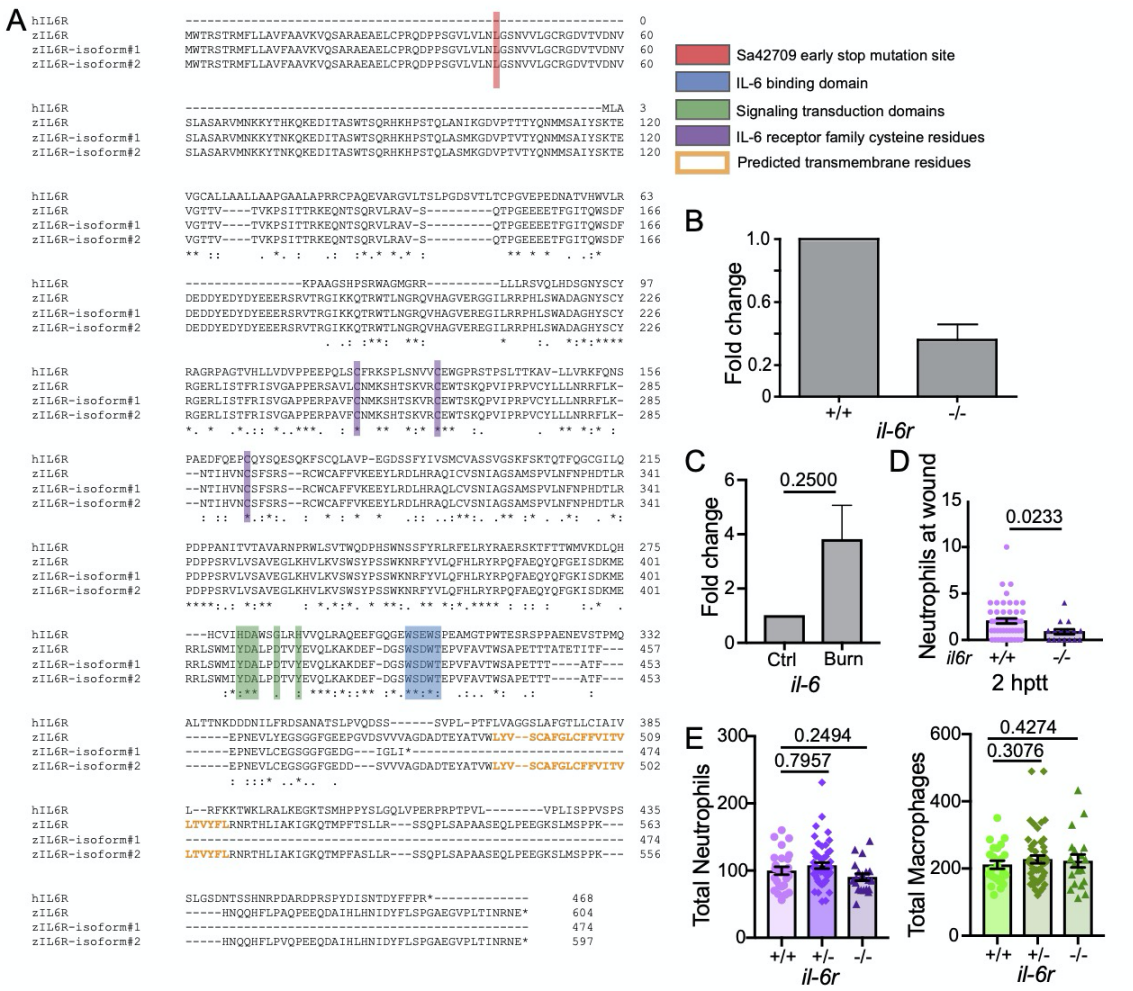

Figure S3: Characterization of zebrafish *il-6r* Sa42709 mutant line. Related to Figure 4. A) Alignment of human (*H. sapiens)* IL-6R protein sequence against zebrafish (*D. rerio*) IL-6R sequence (ENSEMBL) and our two cDNA cloned zebrafish isoform sequences (Isoform #1 and #2). Proteins sequences were aligned using Clustal Omega and relevant domains from the human ortholog are labeled: non-sense mutation site of the Sa42709 zebrafish mutant line (red), IL-6 binding domain (blue), characteristic IL-6 receptor family cysteines residues (purple), conserved signaling transduction residues (green), putative transmembrane domain of zebrafish *il-6r* (orange text). B) *il-6r* mutant larvae express lower amounts of *il-6r* mRNA as determined by RT-qPCR performed using 3dpf *il-6r* $^{+/+}$ or *il-6r* $^{-/-}$ larvae as templates. ΔΔCq analysis was used to calculate fold change in mRNA levels. Bars represent two replicates. Error bar represents SD. C) ΔΔCq analysis was used to calculate fold change in mRNA levels of *il-6* expression from larval tails either without (Ctrl) or with thermal injury (Burn), at 6 hpb. Bars represent arithmetic mean of fold change with SE from 3 independent experiments. p-value was determined by Wilcoxin sign rank test in Prism. D) Quantification of neutrophils recruited to the wound at 2 hours post tail transection (hptt) in *il-6*$^{+/+}$ and *il-6*$^{-/-}$ larvae. Symbols indicate single larvae from two independent replicates. Bars represent arithmetic mean with SE, p-value was calculated using a least squares means analysis in SAS. The total number of E) neutrophils and macrophages quantified in 3 dpf double transgenic larvae. Automated counting (Imaris) was performed on whole larvae MIP images. Data from three independent replicates. Bars represent the

arithmetic mean with SE, and *p*-values were calculated with least squares mean statistical analysis in R, accompanied with Tukey's post-test.

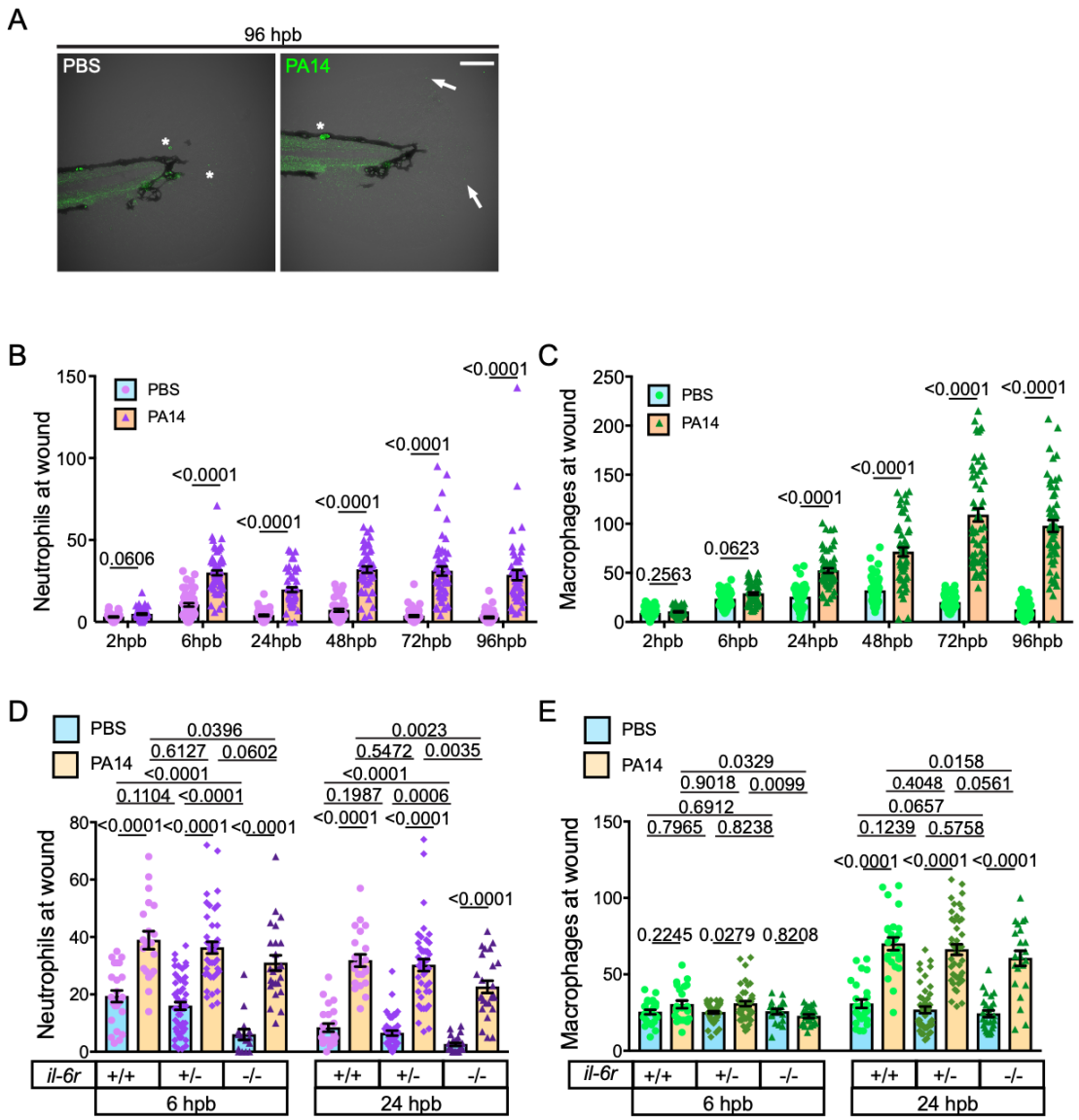

Figure S4: IL-6 receptor is not required for neutrophil recruitment to infected burn wounds. Related to Figure 5. A) Fluorescent micrographs with fluorescently labeled bacteria (PA14) in wildtype tails at 96 hpb illustrating the extensive clearance of bacteria by this time point. Arrows indicate bacteria in infected tails, asterisk denotes non-specific background fluorescence. Scale bar = 200 μm. Quantification of B) neutrophil and C) macrophage recruitment to the burn wound in the presence or absence of *P.aeruginosa* in wildtype larvae up to 96 hpb. Symbols indicate individual larvae. Numbers of D) neutrophils and E) macrophages recruited to the wound in larvae carrying WT (+/+), heterozygous (+/-) or mutant alleles (-/-) for *il-6r.* Symbols represent individual larvae. Presentation of count values (rather than fold change) of the same data as presented in Figure 5 D and E.

TRANSPARENT METHODS

EXPERIMENTAL MODEL AND RESEARCH DETAILS

Zebrafish general procedures

All adult and larval zebrafish (*Danio rerio*) were maintained according to protocols approved by the University of Wisconsin-Madison Institutional Animal Care and Use Committee, in agreement with the guidelines set by the federal Health Research Extension Act and the Public Health Service Policy on the Humane Care and Use of Laboratory Animal, administered by the National Institute of Health Office of Laboratory Animal Welfare.

Collected embryos and larvae were maintained in E3 medium [5mM NaCl (Fisher Scientific), 0.17mM KCl (Dot Scientific), 0.33mM CaCl2 (Acros Organics), 0.33mM MgSO4•7xH2O (Sigma-Aldrich)] with 1% Methylene Blue (Sigma-Aldrich) at 28.5º C. Around 80 embryos were placed on each 90 mm plastic Petri dish. When needed, E3 was supplemented with 0.003% 1-phenyl-2-thiourea (PTU) (Cat#P7629, Sigma-Aldrich), added at 24 hours post fertilization (hpf), to inhibit pigmentation of the larvae. For this project, only 2-3 days post fertilization (dpf) larvae were used for experimental manipulation.

Zebrafish lines

Transgenic lines expressing human fluorescently-tagged histone-2b (H2B) in macrophages (*mpeg1* promoter) or neutrophils (*lyzc* promoter)(von Dassow et al., 2009; Miskolci et al., 2019; Yoo et al., 2012) were outcrossed to create a

double transgenic line *Tg(mpeg1:H2B-EGFP;lyzc:H2B-mCherry)*. The *il-6* receptor (*il-6r*) mutant line Sa42709 was obtained from the Zebrafish International Research Center (Cat# ZL13747.13, ZIRC)(Busch-Nentwich et al., 2012). This line was maintained as heterozygous mutants, and adults were incrossed to obtain heterozygous and homozygous larvae. For qPCR experiments, WT and homozygous mutant adults were created and maintained to obtain the respective alleles in all larvae. *il-6r* mutant line was also outcrossed to the double transgenic line *Tg(mpeg1:H2B-EGFP; lyzc:H2B-mCherry)* to quantify leukocyte recruitment on this mutant background. For second harmonic imaging, transgenic lines *Tg(mpeg1:EGFP)gl22* (Cat#ZL9940, ZIRC)(Ellett et al., 2011) and *Tg(mpx:EGFP)* in *casper* backgrounds (*mpx:GFP/casper* line was a generous gift from Dr. Leonard Zon) were used to image neutrophils and macrophages, respectively. To assess how a neutrophil deficiency can affect burn regeneration we used the previously reported lines *Tg(mpx:mCherry-2A-rac2)* and *Tg(mpx:mCherry-2A-rac2D57N)zf307* (Cat# ZL12825, ZIRC) (Deng et al., 2011).

METHOD DETAILS

Burn procedures

During injury procedures 20-40 3 dpf larvae were transferred to a 35 mm petri dish (Cat# 351008, Falcon) 1% milk-coated dishes and anesthetized with in 2 mL of E3 medium supplemented with 0.2 mg/ml 3-amino benzoic acidethylester (Tricaine; Cat#TRS1 (Pentair), Western Chemical Inc.). A Thermal Cautery Unit (Cat#59005, Stoelting) with a ThermaLite Type E fine palladium electrode #214 (Cat#59010, Stoelting) was used for thermal injury, delivering an approximate

current of 11 Amp for about 1s. Burning of the caudal fin was performed by placing the cautery tip in close proximity to the fin, making sure the tip is not touching the fin. Using a high contrast view of the fin, the burning procedure was stopped before damage reached the notochord. Tail transections were performed with a scalpel size 10 (Cat#4-310-no.10, Integra), also in 35 mm 1% milk-coated dishes containing 2 mL of E3+Tricaine. For live imaging of thermal injury, larvae were mounted in a zWEDGI device (Huemer et al., 2017), maintained in place by adding 1% agarose to the head chamber, and burned as previously described.

Fixation of larvae

All larvae were fixed in 35 mm 1% milk-coated dishes with 2 mL of fixation solution [1.5% Formaldehyde (Cat#1881410, Polysciences, Inc.), 0.1M PIPES (Cat# P1851, Sigma-Aldrich), 1mM MgSO4 (Cat# M7506, Sigma-Aldrich), 2mM EGTA (Cat# E4378, Sigma-Aldrich)] overnight at 4º C (no shaking). Next day larvae were washed 3 times for 5 min with PBS pH 7.4 (Cat# P3813**,** Sigma-Aldrich) and stored in PBS at 4º C until imaging (Yoo et al., 2011a).

Excision of burn tissue

For burn tissue excision, larvae were burn injured or wounded by tail transection at 3 dpf, as described. 24 h later, groups with either burn or wound injuries, were subjected to a second tail transection or to excision of the burn tissue. The cut was done as close to the original injured tissue as possible, taking care in not damaging the notochord. Larvae were fixed 24h later (48h post initial insult)

and neutrophils and macrophages were quantified. Neutrophils and macrophage numbers were normalized to total wound area.

Drug treatments

When indicated, larvae were pre-incubated in drug baths (with Tricaine) 1 h before injury at 28.5º C. After injury, the medium was replaced with fresh medium without Tricaine and larvae were incubated at 28.5º C until fixation at selected timepoints. Drug stock solutions were suspended in DMSO (DPI and SC144) or milliQ H_2O (apyrase) and dissolved to desired concentrations in E3 prior to use. Drug working solutions: Diphenyleneiodonium chloride (DPI) 100µM (Cat#D2926, Sigma), apyrase 50 U/mL (Cat#A6410, Sigma), and SC144 10µM (Cat#506387, EMD Millipore). Control solutions were 1% and 0.2% DMSO (Cat#D2650, Sigma-Aldrich) for DPI and SC144, respectively, and the identical volume of milliQ H_2O for apyrase. In the case of experiments involving DPI, only 1h of pre- and post-injury drug incubation was used. Medium was then replaced with E3.

Acridine orange vital staining

Acridine orange (AO) (Cat#6130, Immunochemistry Technologies) vital staining was performed by incubating larvae at 5.5 hours post-burn for 20 min in 0.0016mg/mL of AO in E3. Larvae were washed 3 times for 5 min with E3+Tricaine prior to imaging (Furutani-Seiki et al., 1996).

Sudan Black staining

For quantification of neutrophil recruitment after a tail transection wound, 3 dpf larvae from a *il-6r* heterozygous incross were wounded with a tail transection (Yoo et al., 2011b), and fixed at 2 hptt in 35 mm 1% milk-coated dishes with 2 mL of fixation solution [4% Paraformaldehyde (Cat# 15710, Electron Microscopy Sciences) in 1x PBS pH 7.4] overnight at 4º C (no shaking). After fixation larvae are washed 3x with 1x PBS pH 7.4. Stain larvae with Sudan Black B (Cat# 199664, Sigma-Aldrich) solution (0.18% w/v stock diluted 1:5 in 70% ethanol, 0.1% phenol (Cat# P4557, Sigma)) for 30 min to 1 hr, at RT and rocking. Wash 1x times with 70% ethanol, 1x with 35%EtOH/PBS then rehydrate samples with 0.1% PBST [0.1% Tween20 (Cat# P1379, Sigma-Aldrich) in 1x PBS pH 7.4]. To clear pigment, incubate larvae in 1% potassium hydroxide/1% hydrogen peroxide solution for approx. 10 min while monitoring the process under a stereomicroscope. Stop the reaction by washing 3x with 0.1% PBST. Transfer to PBS pH 7.4 and store at 4º C. (Le Guyader et al., 2008). After imaging with wide field microscopy (see below), single larvae were genotyped as described below.

il-6r mutant genotyping

The *il-6r* Sa42709 mutant line was genotyped by Restriction Fragment Length Polymorphism (RFLP). Genomic DNA (gDNA) extraction was performed by incubating single larvae in 100 μL of 50 mM NaOH (Cat# S8045, Sigma-Aldrich) at 95º C in a shaking block (1100 rpm) for 10 min and 20 min, for live or fixed larvae, respectively. Samples were cooled to 4º C. Solution was neutralized with 10 μL of 1 M Tris-HCl pH8 (Cat#BP152-500, Fischer Scientific). Tubes were centrifuged at max speed for 10 min, and 1 μL of the supernatant was

used as template for subsequent reactions. Polymerase Chain Reaction (PCR) was performed using a 25 μL total volume reaction with GoTaq Green Master Mix 2x (Cat# M7123, Promega), using primers IL6R gen F; 5'-AAATCTTCATCAGATCCTCCTTCTGGAGCTT-3, and IL6R gen R; 5'-AGCTGGCAGTGATGTCTTC-3'. PCR cycler program was performed as suggested by the manufacturer (Promega), with a primer melting temperature of 53º C was used, and a total of 30 cycles. Digestion of PCR amplicons with DdeI (Cat#R0175S, New England Biolabs) was carried out by adding 3μL of enzyme mix [0.3μL of DdeI, 0.3μL of 10x CutSmart Buffer, and 2.4 μL of milliQ H_2O] directly to the PCR mix. Samples were incubated O/N at 37º C, and resolved at 90V on a 2.5% agarose gel (Cat# V3125, Promega).

RT-qPCR

To prepare samples for *il-6r* analysis, total RNA from 5 larvae (*il-6r*$^{+/+}$ or *il-6r*$^{-/-}$) was extracted using TRIzol reagent (Cat#15596018**,** Invitrogen) following standard manufacturer's directions. For for *il-6* analysis, 50 WT larvae were burned as described and tails were cut and collected at 6 hpb in TRIzol reagent, followed by extraction of total RNA using RNAqueous Total RNA Isolation kit (Cat#AM1931, Ambion) following standard manufacturer's directions. cDNA was synthesized with SuperScript III First-Strand Synthesis System kit (Cat#18080051**,** Invitrogen), normalizing for equal amounts of total RNA per sample, using oligo-dT primers, and following standard manufacturer's directions. Using this cDNA as template, quantitative PCR was performed using FastStart Essential DNA Green Master Mix (Cat#6402712001, Roche), following standard manufacturer's directions. A LightCycler96 thermocycler

(Roche) was used, with a programmed melting temperature of 58º C and 60º C for *il-6r* and *il-6*, respectively, and the reaction was run for 40 cycles. The following primers were used:

IL6R qPCR F; 5'-TTTATGTCCTGCAGTTCCATCT-3',

IL6R qPCR R; 5'-ACAGTCGTCTCTCCATCTTGT-3',

IL6 qPCR F; 5'-TCAACTTCTCCAGCGTGATG-3',

IL6 qPCR R; 5'-TCTTTCCCTCTTTTCCTCCTG-3' (Varela et al., 2012),

ef1a qPCR F; 5'-TGCCTTCGTCCCAATTTCAG-3',

ef1a qPCR R; 5'-TACCCTCCTTGCGCTCAATC-3' (Oehlers et al., 2010).

Data were normalized to ef1α, and level fold changes were calculated using the ΔΔCt method (Livak and Schmittgen, 2001).

il-6r mRNA rescue

To rescue the *il-6r* mutant phenotype, zebrafish *il-6r* was amplified from 3dpf WT larvae cDNA using Phusion High-Fidelity DNA polymerase (Cat# F530S, Thermo-Fisher), following standard manufacturer's directions. Two separate reactions were done to avoid non-specific amplification. First, using the primers IL6R cDNA F; 5'-ATGTGGACCCGATCTACACGC-3', and IL6R cDNA R; 5'-TTCATTTCTGTTTATTGTCAATGGCAC-3', the primer melting temperature used was 64.2º C, and this reaction was run for 25 cycles. Reaction products were separated on a 1% agarose gel and a band of roughly 2 kbp was cut and purified using NucleoSpin Gel and PCR Clean-up kit (Cat# 740986.20, Macherey-Nagel). Next, using this as template, another PCR reaction was performed using primers IL6R pCS2 F; 5'-CTTTTTGCAGGATCCGCAAACATGTGGACCCGATCTACACGC-3' and IL6R

pCS2 R; 5'-GAGGCCTTGAATTCCTTCATTTCTGTTTATTGTCAATGGCAC-3'. This was done as previously, but for 30 cycles. Amplicon was purified from a 1% agarose gel and cloned by homologous recombination into pCS2+8 (Cat#34931, Addgene) using In-Fusion HD cloning kit (Cat#638911, Clonetech). Recombination products were transformed into Stellar competent cells (Cat# 636766, Takara) following manufacturer's directions. Positive colonies were selected, and mRNA was transcribed using mMessage mMachine SP6 in vitro transcription kit (Cat#AM1340, Ambion). mRNA was purified using Qiagen RNA Easy mini kit (Cat#74104, Qiagen). Double transgenic adults *Tg(mpeg1:H2B-EGFP;lyzc:H2B-mCherry)* carrying either WT or *il-6r*$^{-/-}$ alleles were incrossed, and at 1-cell stage embryos were injected with 3 nL of *il-6r* mRNA (isoform #1) solution at 50 ng/ul. Injected larvae were burned at 2 dpf and fixed at 6 hpb.

Neutrophil deficient larvae

To measure the influence of neutrophils on fin regeneration, 3 dpf *Tg(mpx:mCherry-2A-rac2D57N)* and *Tg(mpx:mCherry-2A-rac2)* larvae were anesthetized and burned as above. Following injury, medium was changed to E3. Larvae were incubated at 28.5º C then fixed at 72 hpb as described above. Regenerated area was quantified using FIJI as described below.

***Pseudomonas aeruginosa* culture preparation and infection of burn wounds**

P. aeruginosa strain PA14-YFP was acquired as a gift from Dr. Nancy Keller (University of Wisconsin-Madison)(Wang et al., 2011). Infection of injured tissue

was done as described previously, with minor modifications (Miskolci et al., 2019). Liquid culture of LB+Gentamicyn was inoculated with a single colony and grown overnight in at 37º C and 250 rpm. The culture was then diluted 1:5 and grown for an additional 1.25-2.5 hours in a 250 mL Erlenmeyer Flask. OD (600nm) was measured by diluting the culture in PBS at a 1:1 ratio, until reaching an OD of 0.2-0.3. Bacteria were then pelleted (2 min at 3,000 rcf), and washed 3 times 1 mL of filter-sterile PBS. The final bacterial pellet was resuspended in 100 μL sterile PBS, for a final concentration of $8x10^7$ CFU/mL. Burn was done as described previously, with minor modifications. Larvae were injured in a 60mm tissue culture treated dishes (Cat#430589, Corning) containing 5 mL of E3+Tricaine. To avoid wound closure all larvae were burned in less than 2 min per plate. Total volume of bacterial suspensions or sterile PBS was added to the plates immediately following burn. Plates were placed on a rocker at minimum speed (to avoid further damage to the larvae skin) and incubated for 1 hour at room temperature. Following incubation, larvae were washed carefully with 5 mL of E3 five times before being placed in the incubator at 28.5° C. Larvae were fixed at specific timepoints and leukocytes were quantified as described below.

Confocal microscopy image acquisition

All live imaging procedures were performed at temperatures between 23 to 27º C. Confocal imaging was done on a Zeiss Axio Observer.Z1 microscope (Zeiss) with EC Plan-Neofluar NA 0.3/10x objective lens (Zeiss). The spinning disc module corresponds to a CSU-X1 (Yokogawa), coupled to an EMCCD evolve 512 camera (Photometrics). This set up was run by Zen 2 acquisition software

(Zeiss). Laser power, exposure time, and camera gain were defined for each set of experiments. For imaging macrophage and neutrophil responses to a burn injury in the caudal fin, approximately 150 μm depth z-series (8.5 μm step size) of each larva were taken approximately every 2 min. For total number of leukocytes, fixed 3dpf larvae were immobilized in the zWEDGI (no agarose), and 6x1 tile regions were collected for each larva, using 200 μm depth z-series (10 μm step size) and 10% image overlap. For acridine orange imaging, 2x1 tile regions were adjusted for each larval caudal fin, using 180 μm depth z-series (5 μm step size) and 10% of image overlap. Stitching of tiles was done on Zen 2 (Zeiss) using default settings. To image the presence of PA14-YFP in fin burns, a laser-scanning confocal microscope Olympus FluoView FV1000 (Olympus) with a NA0.40/10x objective (Olympus) was used. Images were 800x800 pix in size and acquired using a pinhole of 80 μm diameter. Fluorescence channel (488 nm) and DIC images were acquired by sequential line scanning.

Widefield microscopy image acquisition

Images were taken at a magnification of 112x using a Axio Zoom.V16 zoom microscope (Zeiss) with a Plan-Neofluar Z 1x lens (Zeiss), coupled with a AxioCam MRm camera (Zeiss). This set up was run by Zen 2012 acquisition software (Zeiss). Fluorescence intensity and exposure time were defined for each set of experiments. For fixed burn macrophage and neutrophil recruitment experiments, larvae tails were amputated from the larvae body (so the tissue lays flat) prior to imaging. Sudan Black stained embryos were imaged using brightfield microscopy on a SMZ1500 zoom stereomicroscope (Nikon) with a WD 54 HR Plan Apo1X lens (Nikon). This instrument was controlled by NIS-

Elements D acquisition software. Exposure time was defined for each set of experiments.

Multiphoton microscopy image acquisition

Image data were collected on a custom-built multiphoton laser scanning microscope (LeBert et al., 2018) and lab-developed acquisition software at the UW Laboratory for Optical and Computational Instrumentation. Images were collected using a 20x air lens (Nikon, 20X VC, 0.75 NA) and a H7422P-40 GaAsP photomultiplier (Hamamatsu). The Ti:Sapphire laser (Coherent Ultra) was set at 890 nm for excitation. For detection of the GFP fluorescence a 520/30 nm emission filter (Semrock) was used, while a 445/20 nm bandpass emission filter (Semrock) was used for Second Harmonic Generation (SHG) detection. Anesthetized 3 dpf larvae (*Tg(mpx:EGFP)* or *Tg(mpeg1:EGFP)gl22* in *casper* background) were loaded into a zWEDGI device (Huemer et al., 2017). Caudal fins were thermally injured then imaged for 20 to 24 hours, starting at approximately 1.5 hpb. Microscope stage temperature was maintained at 25 to 28º C for the duration of the experiment. Data were collected as z-stacks at each time point, with 4 microns between z-sections and approximately 30 min between time points. Spectral channels (via filters) were collected sequentially for each z-stack, with GFP fluorescence collected first. Brightfield images were collected simultaneously with the SHG collection, using a transmission photodiode detector (Bio-Rad).

QUANTIFICATION AND STATISTICAL ANALYSIS

Leukocyte recruitment

For neutrophil and macrophage recruitment in fixed tissue, images were quantified using Zen 2.3 Blue Edition (Zeiss) or FIJI (Schindelin et al., 2012) using the event counter tool for each cell type, or the area tool for regeneration experiments. Only nuclei were counted, rejecting small fragmented or phagocytosed nuclei when possible. To quantify recruitment, a burn area was defined as the entire fin tissue (excluding notochord tissue) posterior from the artery loop. For experiments quantifying leukocyte recruitment in *il-6r* mutants, quantification was performed prior to genotyping. For *il-6r* mutant rescue experiments, genotype was known prior to quantification.

Regeneration

Area of regeneration was measured using Zen 2.3 Blue Edition (Zeiss) or FIJI (Schindelin et al., 2012) by outlining the entire fin tissue posterior to the tip of the notochord. Regeneration length was defined as a straight line starting from the end and parallel to the notochord to the end of the caudal fin or burned tissue. For experiments quantifying regenerate area in *il-6r* mutants, quantification was performed prior to genotyping.

Leukocyte infiltration into burn tissue

Infiltration distance of leukocytes into the burn tissue was measured using Zen 2.3 Blue Edition (Zeiss), using the last frame from 6 hour-long time-lapse recordings. A perpendicular line was drawn at the end of the notochord, the distance from this line to the edge of a neutrophil and macrophage nuclei was measured. Only nuclei posterior from this line were measured and any that overlapped with the line were count as 0 μm distance.

Total leukocyte count

Total macrophage and neutrophil numbers were quantified using spot analysis tool from Imaris imaging analysis software (Bitplane). Spots were defined as particles with 10 μm and 20 μm of X/Y and Z diameter, respectively. Imaris quality filter was set for each tile image, between 200-300 for neutrophils, and 300-500 for macrophages.

Tracking of migrating leukocytes

For tracking of neutrophil and macrophage speed, cells were tracked using the Imaris spot function, where estimated spot size was defined as 10 μm. Imaris quality filter was set to 500 or above. Max distance and max gap parameters were defined as 50 μm and 5 frames, respectively. Single tracks were curated after software detection. Five randomly selected individual tracks that crossed the plane of the notochord were selected in each larvae imaged across two replicates. The time that the cell crossed the plane of the notochord was set to 0 and speed was quantified for 50 min in both the trunk of the fish ($t < 0$) and the wound area ($t > 0$). Mean cell speed for each time point was determined for both neutrophils and macrophages.

Leukocyte residency in burn tissue

For assessing residency of neutrophils and macrophages in the burn area, track images were made from the tracks defined above. The recordings were split into three sections: 0-2 hr, 2-4 hr and 4-6 hr, with cumulative tracks within each time segment made by defining the dragon tail of the track to fill from the

terminal time point (e.g. 6 hr) to the initial time point (e.g. 4 hr) in Imaris. This was performed separately for each cell type. Greyscale images of these tracks, along with a single DIC image of the segment ending time point were then exported. Subsequent processing and analysis was conducted using FIJI software. The track images were converted to binary images. The DIC images were used to generate 2 regions of interest, the wound area - defined by the area extending from a line perpendicular to the distal end of the notochord to the edge of the tissue – and the non-wound area – defined as the area incorporating the trunk area extending from the line perpendicular to the end of the notochord anteriorly along the trunk the same distance as the length of the wound area so that, for a given tail, the two regions encompassed similar, though not identical, areas. These two regions of interest (ROIs) were then overlaid onto each (neutrophil or macrophage) of the binary track images and FIJI determined the percentage of each ROI that was occupied by tracks. This percent area value for the wound region was divided by the percent area value for the non-wound region to control for larvae to larvae variation in leukocyte number.

Leukocyte residency in collagen areas

For second harmonic generation images an initial processing to separate the multiple spatial location of larvae into single larva time-lapse data sets was performed in FIJI to generate merged data sets containing brightfield, GFP and SHG images. Imaris (Bitplane) was used to generate 3D reconstructions of the merged data sets and surface rendering of the macrophage and neutrophil fluorescence. The surface rendered macrophages or neutrophils were manually

categorized according to location at select time points and total volumes for specified cell types in each region were for each time point were determined by Imaris. Cells not completely in the field of view, those that were stationary over several timepoints or statically overlapping bright SHG signal were not included in the analysis. As an assessment of the change of total volumes for each cell type within different time windows after thermal injury, the volume measurement for each of the time points within a time window were used to calculate a slope (Microsoft Excel v16.37) for that time window for each larva.

Video preparation:

Time-lapse files were analyzed and exported from Imaris as MP4 video files. These files were then imported into FIJI using the FFMPEG plugin (http://fiji.sc/~schindelin/ffmpeg-plugins/). Videos were then labeled and combined into one. First and last frames were duplicate and expanded into 20 frames to demark respective regions on those time points. Using DIC channel as a reference, burn tissue areas was drawn using a segmented line. Finally, all segments were concatenated into one video, and exported as an 18fps AVI uncompressed file. Videos were then compressed and formatted into a smaller MP4 file. Relative acquisition time and scale bar were originally added in Imaris. 3D reconstructions of a single time point, for neutrophils and for macrophages, of the data presented in Figure 2 were animated in Imaris and exported as individual AVI files. The AVI files were converted to TIF files in FIJI, concatenated into a single video and annotated using the Annotation to Overlay V1.4 macro (https://www2.le.ac.uk/colleges/medbiopsych/facilities-and-services/cbs/AIF/software-1/imagej-macros). Video was exported at a 15fps

frame rate as an AVI with JPEG compression. Further compression to MP4 format was accomplished using Handbrake video conversion software (https://handbrake.fr/).

Human burn skin expression data

To analyze gene expression data on human burn skin samples, we used the previously published expression dataset from Karim et al, 2018, and followed a similar analysis pipeline. Briefly, two genesets were used in order to compare to human expression data. In the case of *IL-6* related genes, an available human *IL-6* pathway geneset was used (GSEA; BioCarta; URL:https://www.gsea-msigdb.org/gsea/msigdb/cards/BIOCARTA_IL6_PATHWAY). In case of neutrophil genes, a curated list of genes from two separate sources was obtained. Using Geneontolgy (Ashburner et al., 2000; The Gene Ontology Consortium, 2019) we used the search term “neutrophil” to find genes related to neutrophil migration, activation, extravasation, homeostasis, and surface markers. This list was compared against a previously published list of neutrophil-related genes upregulated in wound healing(Theilgaard-Mönch et al., 2004) (GSEA; URL: https://www.gsea-msigdb.org/gsea/msigdb/cards/THEILGAARD_NEUTROPHIL_AT_SKIN_WOUND_UP). Repeated genes from the two sources were eliminated, thus generating a list of 140 genes. Both genesets were then compared against the human expression data from burn patients (Karim et al., 2019), and single sample geneset enrichment analysis (ssGSEA) was done to generate normalized enrichment scores as previously described (Barbie et al.,

2009). Full gene list, gene analysis, and ssGSEA scores are listed in the Data S1 file.

Statistics

Graphs: All graphed data in the main text represent at least 3 independent replications of the experiment, unless otherwise noted in the figure legend, and were generated using Prism 7.0 (GraphPad). For all graphs, symbols represent individual data points (defined in the figure legends), the columns indicate the arithmetic mean and the error bars are the corresponding standard error, with p-values listed above the relevant comparisons. Significance level was determined at $p < 0.05$. Additional statistical information, such as n values, the least square means and standard errors used for comparison and the 95% confidence intervals for all data in the main text have been provided in Table S1.

Analyses: Except for human expression analysis, total larva leukocyte counts and RT-qPCR data, statistical tests were performed using SAS/STAT 9.3 (SAS Institute Inc.). Analysis of variance was conducted using SAS general linearized mixed model to account for variation due to fixed effects and random effects. For experiments where measurements were taken on the same sample at multiple time points, a repeated measures statement was incorporated into the analysis model. For the distance measurements of single leukocytes, a nested statement was incorporated in the analysis model for cells with the same larvae. For mean leukocyte speed, analysis was performed using the mean speed value within a tail. A square root transformation was performed on skewed data sets to prior to analysis improve normality of residuals. For analysis of mean slope data, an

analysis of ranks was performed due to non-normality of residuals. Human RNA expression data were compared using Prism 8 (GraphPad), with normalized enrichment scores were plotted and analyzed using ANOVA to compare all three groups, followed by a pairwise comparison with Tukey's correction. Total larva leukocyte counts *p*-values were calculated with least squares mean statistical analysis in R (The R Project), accompanied with Tukey's post-test, while RT-qPCR data was compared using Wilcoxin Signed Rank test in Prism 7 (GraphPad).

SUPPLEMENTAL REFERENCES

Ashburner, M., Ball, C.A., Blake, J.A., Botstein, D., Butler, H., Cherry, J.M., Davis, A.P., Dolinski, K., Dwight, S.S., Eppig, J.T., et al. (2000). Gene ontology: tool for the unification of biology. The Gene Ontology Consortium. Nat. Genet. *25*, 25–29.

Barbie, D.A., Tamayo, P., Boehm, J.S., Kim, S.Y., Moody, S.E., Dunn, I.F., Schinzel, A.C., Sandy, P., Meylan, E., Scholl, C., et al. (2009). Systematic RNA interference reveals that oncogenic KRAS-driven cancers require TBK1. Nature *462*, 108–112.

Busch-Nentwich, E., Kettleborough, R., Harvey, S., Collins, J., Ding, M., Dooley, C., Fenyes, F., Gibbons, R., Herd, C., Mehroke, S., et al. (2012). Sanger Institute Zebrafish Mutation Project phenotype and image data submission.

von Dassow, G., Verbrugghe, K.J.C., Miller, A.L., Sider, J.R., and Bement, W.M. (2009). Action at a distance during cytokinesis. J. Cell Biol. *187*, 831–845.

Deng, Q., Yoo, S.K., Cavnar, P.J., Green, J.M., and Huttenlocher, A. (2011). Dual roles for Rac2 in neutrophil motility and active retention in zebrafish hematopoietic tissue. Dev. Cell *21*, 735–745.

Ellett, F., Pase, L., Hayman, J.W., Andrianopoulos, A., and Lieschke, G.J. (2011). mpeg1 promoter transgenes direct macrophage-lineage expression in zebrafish. Blood *117*, e49-56.

Furutani-Seiki, M., Jiang, Y.J., Brand, M., Heisenberg, C.P., Houart, C., Beuchle, D., van Eeden, F.J., Granato, M., Haffter, P., Hammerschmidt, M., et al. (1996). Neural degeneration mutants in the zebrafish, Danio rerio. Development *123*, 229–239.

Le Guyader, D., Redd, M.J., Colucci-Guyon, E., Murayama, E., Kissa, K., Briolat, V., Mordelet, E., Zapata, A., Shinomiya, H., and Herbomel, P. (2008). Origins and unconventional behavior of neutrophils in developing zebrafish. Blood *111*, 132–141.

Huemer, K., Squirrell, J.M., Swader, R., LeBert, D.C., Huttenlocher, A., and Eliceiri, K.W. (2017). zWEDGI: Wounding and Entrapment Device for Imaging Live Zebrafish Larvae. Zebrafish *14*, 42–50.

Karim, A.S., Yan, A., Ocotl, E., Bennett, D.D., Wang, Z., Kendziorski, C., and Gibson, A.L.F. (2019). Discordance between histologic and visual assessment of tissue viability in excised burn wound tissue. Wound Repair Regen. *27*, 150–161.

LeBert, D., Squirrell, J.M., Freisinger, C., Rindy, J., Golenberg, N., Frecentese, G., Gibson, A., Eliceiri, K.W., and Huttenlocher, A. (2018). Damage-induced reactive oxygen species regulate vimentin and dynamic collagen-based projections to mediate wound repair. Elife *7*.

Livak, K.J., and Schmittgen, T.D. (2001). Analysis of relative gene expression data using real-time quantitative PCR and the 2(-Delta Delta C(T)) Method. Methods *25*, 402–408.

Miskolci, V., Squirrell, J., Rindy, J., Vincent, W., Sauer, J.D., Gibson, A., Eliceiri, K.W., and Huttenlocher, A. (2019). Distinct inflammatory and wound healing responses to complex caudal fin injuries of larval zebrafish. Elife *8*.

Oehlers, S.H.B., Flores, M.V., Hall, C.J., O'Toole, R., Swift, S., Crosier, K.E., and Crosier, P.S. (2010). Expression of zebrafish cxcl8 (interleukin-8) and its receptors during development and in response to immune stimulation. Dev. Comp. Immunol. *34*, 352–359.

Schindelin, J., Arganda-Carreras, I., Frise, E., Kaynig, V., Longair, M., Pietzsch, T., Preibisch, S., Rueden, C., Saalfeld, S., Schmid, B., et al. (2012). Fiji: an open-source platform for biological-image analysis. Nat. Methods *9*, 676–682.

The Gene Ontology Consortium (2019). The Gene Ontology Resource: 20 years and still GOing strong. Nucleic Acids Res. *47*, D330--D338.

Theilgaard-Mönch, K., Knudsen, S., Follin, P., and Borregaard, N. (2004). The transcriptional activation program of human neutrophils in skin lesions supports their important role in wound healing. J. Immunol. *172*, 7684–7693.

Varela, M., Dios, S., Novoa, B., and Figueras, A. (2012). Characterisation, expression and ontogeny of interleukin-6 and its receptors in zebrafish (Danio rerio). Dev. Comp. Immunol. *37*, 97–106.

Wang, Y., Wilks, J.C., Danhorn, T., Ramos, I., Croal, L., and Newman, D.K. (2011). Phenazine-1-carboxylic acid promotes bacterial biofilm development via ferrous iron acquisition. J. Bacteriol. *193*, 3606–3617.

Yoo, S.K., Starnes, T.W., Deng, Q., and Huttenlocher, A. (2011a). Lyn is a redox sensor that mediates leukocyte wound attraction in vivo. Nature *480*, 109–112.

Yoo, S.K., Starnes, T.W., Deng, Q., and Huttenlocher, A. (2011b). Lyn is a redox sensor that mediates leukocyte wound attraction in vivo. Nature *480*, 109–112.

Yoo, S.K., Lam, P., Eichelberg, M.R., Zasadil, L., Bement, W.M., and Huttenlocher, A. (2012). The role of microtubules in neutrophil polarity and migration in live zebrafish. J. Cell Sci. *125*, 5702–5710.